This is the accepted manuscript made available via CHORUS. The article has been published as:

Two-proton decay from math xmlns="http://www.w3.org/1998/Math/MathML">mi>α/mi> /math>-cluster states in math xmlns="http://www.w3.org/1998/Math/MathML">mmultiscripts>mi mathvariant="normal">C/mi> mprescripts>/mprescripts>none>/none>mn>10/mn>/mmultiscripts>/math> and math xmlns="http://www.w3.org/1998/Math/MathML">mmultiscripts>mi mathvariant="normal">N/mi> mprescripts>/mprescripts>none>/none>mn>11/mn>/mmultiscripts>/math>

R. J. Charity, L. G. Sobotka, T. B. Webb, and K. W. Brown

Phys. Rev. C **105**, 014314 — Published 19 January 2022

DOI: 10.1103/PhysRevC.105.014314

Two-proton decay from alpha-cluster states in ^{10}C and ^{11}N

R. J. Charity,[1] L. G. Sobotka,[1,2] T. B. Webb,[2] and K. W. Brown[1,3]

[1]*Department of Chemistry, Washington University, St. Louis, Missouri 63130, USA*
[2]*Department of Physics, Washington University, St. Louis, Missouri 63130, USA*
[3]*National Superconducting Cyclotron Laboratory, Michigan State University, East Lansing, Michigan 48824, USA*

Two-proton decay from excited states in ^{10}C and ^{11}N has been characterized from an analysis of the $2p$+2α and $3p$+2α exit channels. Data from four previously-published invariant-mass studies associated with inelastic excitation, multi-nucleon knockout, and neutron pickup reactions have been considered. A rotational band in ^{10}C was identified built on the second 0^+ state which has strong α-cluster molecular structure. The members of this band were tentatively identified up to J^π=4^+ and all identified states have a prompt $2p$ decay branch. The spins of the 0^+ and 2^+ members were deduced from comparisons of the momentum correlations in their $2p$ branches to those from known $2p$ emitters. The 2^+ and the tentative 4^+ members are both above the α threshold and exhibit large reduced decay widths for α emission. This band exhibits a similar moment of inertia to its analog in the mirror nucleus ^{10}Be. Evidence is also presented for a molecular band in ^{11}N built on the second $3/2^-$ state which $2p$ decays. Tentative members of this band have been assigned up to J^π=$9/2^-$ and their excitation energies also match their likely analogs in the mirror nucleus ^{11}Be.

I. INTRODUCTION

Ground-state $2p$ emission has been observed in even-Z isotopes beyond the proton drip line. This prompt process is often call "true" $2p$ emission if there is no (Z-1,A-1) intermediate state energetically available for $1p$ decay or democratic if such an intermediate state is available but very wide [1, 2]. The latter are typically restricted to light isotopes where the Coulomb barriers to proton emission are small. Both types of $2p$ decay involve similar physics and are treated within the same theoretical frameworks [3–6].

The phenomena of $2p$ emission is not confined to ground states and some of the ground-state $2p$ emitters also have excited states where a rich and complex evolution from prompt to sequential $2p$ decay is observed with increasing excitation energy [7–9]. Moreover, $2p$ emission is not expected to be restricted to the particle-unbound even-Z isotopes. For the odd-Z nuclides both inside and beyond the proton drip line, it is possible that excited states can $2p$ decay. For instance in ^{12}N, the isobaric analog of the $2p$ emitter ^{12}O$_{g.s.}$ was found to undergo $2p$ decay [10] with the same momentum correlations between the decay products as measured for ^{12}O$_{g.s.}$ [9]. The isobaric analog state of ^{8}C$_{g.s.}$ in ^{8}B was also observed to be a $2p$ emitter [11]. The ^{8}C ground state undergoes two sequential steps of $2p$ decay [12, 13]. Two-proton decay of the ^{16}Ne$_{g.s.}$ isobaric analog state in ^{16}F was searched but not found in Ref. [14].

Apart from these analogs of ground-state $2p$ emitters, observations of $2p$ decays of excited states are quite sparse with only the $2p$ decay of two ^{10}C excited states [15] being reasonably well characterized. In this work, we will continue the study of $2p$ decay from ^{10}C excited states and search for $2p$ decay from excited states in its odd-Z neighbor ^{11}N which is located just beyond the proton drip line. Apart from the lowest excited states in these two nuclei, the decay of their states is expected to lead to highly-fragmented exit channels, i.e. $2p$+2α and $3p$+2α respectively. Possible decay paths leading to these channels can be quite varied. These decay paths can include prompt and sequential $2p$ decay as steps in a series of decays leading to the final exit channels. To characterize these, one has to isolate particle-unstable intermediate states produced during these series of decays. Some experience of this has been acquired from the analysis of the $4p$+α exit channel of ^{8}C [12, 13] and the $4p$+2α exit channel of ^{12}O [9], but further refinement is needed to isolate weak channels.

Some of the $2p$ emitters observed in this work will be shown to possess strong α-cluster structure. Alpha-clustered states are found in light nuclei typically near the α-emission threshold. The iconic case is the ground-state of ^{8}Be that has a shape, as calculated in the *ab initio* Green's Function Monte Carlo formalism, which looks like two α particles joined together [16]. This deformed structure is associated with a rotational band with 2^+ and 4^+ members. One can add nucleons to σ and π molecular-like orbits associated with these alpha particles to produce other cluster configurations. Adding a neutron to the π orbital produces the ground state of ^{9}Be which also anchors a rotational band. Molecular bands are also known in ^{9}B, ^{10}Be, and ^{12}Be [17–19]. When the nucleons are added to σ orbits, this tends to push the two α particles apart producing more deformed configurations [17].

In this work we will make use of four data sets using Si and CsI(Tl) detectors from the HiRA apparatus [20] to study the states associated with the $2p$+2α and $3p$+2α exit channels. In the first lowest-energy data set obtain from an experiment at the Texas A&M cyclotron, the $2p$+2α channel is produced following the inelastic scattering of an E/A=10.7-MeV ^{10}C beam on 14.1-mg/cm^2 ^{9}Be and 13.4-mg/cm^2 ^{12}C targets. In this experiment, charged particles were detected in an array of four Si-Si E-ΔE telescopes located 14 cm downstream of the target covering polar angles from 5° to 33°. Data from this experiment have previously been published in Refs. [15, 21, 22] where details of the setup and calibrations can be found. A total of 6x10^4 $2p$+2α events were

detected.

Three higher-energy data sets are included all utilizing almost identical HiRA setups in experiments perform at the National Superconducting Cyclotron Laboratory at Michigan State University. These include a mixed ^{15}O (≈89%, E/A=48.1 MeV) plus ^{17}Ne (≈11%, E/A=58.2 MeV) secondary beam [8, 14, 23–25], a ^{13}O secondary beam of E/A=65.4 MeV [9, 26–29] and a E/A=67-MeV ^{9}C secondary beam [11–13, 24]. These secondary beams were incident of a 1-mm-thick ^{9}Be target and charged particles were detected in 14 Si-CsI(Tl) E-ΔE telescopes located 80 cm downstream of the target covering polar angle from 2.1° to 12.4°. With the A >10 secondary beams, excited states in ^{11}N and ^{10}C were produced via multi-nucleon knockout reactions either directly or indirectly following sequential charged-particle emission. Only the ^{13}O data set populated the $3p$+2α exit channel with significant yield (3x10^5 events). For the ^{9}C secondary beam, ^{10}C states were populated via neutron pickup reactions and only 1.2x10^4 $2p$+2α events were detected. The ^{13}O data set has the highest $2p$+2α statistics with 2x10^6 events followed by the ^{15}O/^{17}Ne data set with 8x10^5 events.

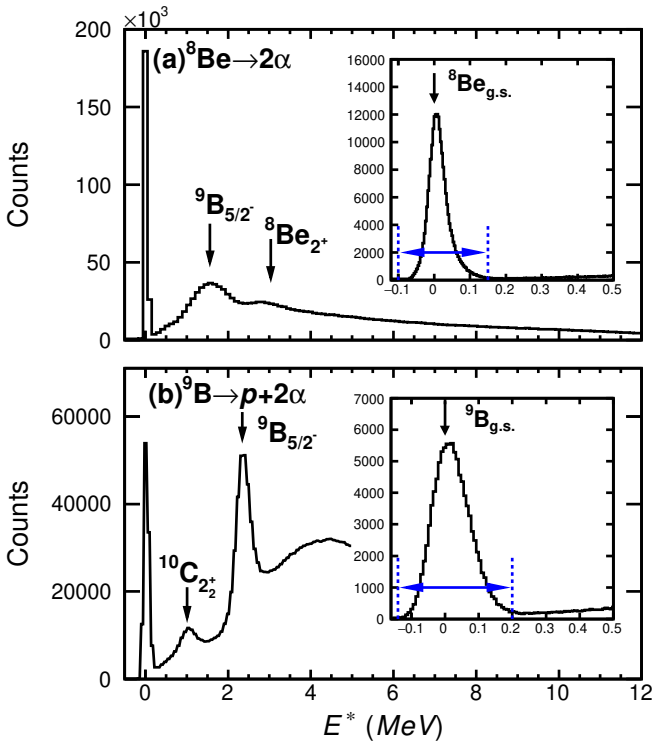

FIG. 1. Distributions of ^{8}Be and ^{9}B excitation energy E^* for (a) 2α and (b) p+2α subevents in the detected $2p$+2α events from the ^{13}O data set. The insets in both panels show an expanded view of the ^{8}Be and ^{9}B ground-state peaks where the bin size on the energy axis is decreased. The sources of the observed peaks are indicated. The figure also demonstrates that correlations from decay of states can be visible in the invariant-mass distributions of the subevents. For example the peak at ≈1 MeV in (b) is produced by the decay of the second 2_2^+ state of ^{10}C. This state proton decays to the ground state of ^{9}B. This peak is produced by the subevent comprised of the first-emitted proton and the α particles produced in the decay of ^{9}B. Similarly the $5/2^-$ state in ^{9}B produces a broad peak in the invariant-mass of the 2α subevents in (a).

II. ^{10}C STATES DECAYING TO THE $2p$+2α EXIT CHANNEL

The $2p$+2α exit channel can have contributions from ^{10}C states that decay by many different decay paths. For example, α and proton decays lead to ^{6}Be and ^{9}B states which are both particle unstable, even in their ground states, and their decay leads to this final exit channel. In addition, two-proton decay leads to ^{8}Be states which breakup into two α particles again producing the $2p$+2α channel. By selecting events associated with different intermediate states, we are better able to separate states which decay via these different paths. This selection on intermediate states helps isolate levels produced with low intensity. In general, it is quite difficult to select out a particular intermediate state. For example, one could attempt to find events associated with a ^{6}Be$_{g.s.}$ intermediate state which has a small decay width of 96 keV by looking at the invariant mass of the p+2α subevents. As all $2p$+2α events produce two different p+2α subevents, then even if all events are associated with one ^{6}Be$_{g.s.}$ intermediate state, the p+2α invariant-mass spectrum will still have a significant background under the ^{6}Be$_{g.s.}$ peak. Attempts to subtract this background by gating on a neighboring region of the $2p$+α spectra next to the ^{6}Be$_{g.s.}$ peak are frustrated by the fact that a single event can contribute to both the ^{6}Be$_{g.s.}$ peak and to this background region from its different subevents.

However, there are two intermediate states which can be gated on very cleanly, namely ^{8}Be$_{g.s}$ and ^{9}B$_{g.s.}$ as they are very narrow and located just above threshold where background contributions to the invariant mass from all sources are typically negligible. Figure 1 shows the excitation-energy spectra of the 2α and p+2α subevents where the resonance peaks associated with these ground states are very prominent. The regions around the ground-state peaks has been expanded in the insets showing that the background under these peaks is small and the gates utilized in the subsequent analysis are displayed. As ^{9}B$_{g.s.}$ decays sequentially through ^{8}Be$_{g.s.}$, these gates can be used to subdivide all events into three groups; (a) those that decay though ^{9}B$_{g.s.}$ and hence also through ^{8}Be$_{g.s.}$, (b) those that decay through ^{8}Be$_{g.s.}$, but not through ^{9}B$_{g.s.}$, (c) and those that did not decay through ^{8}Be$_{g.s.}$.

Invariant-mass distributions for these three subdivisions of the events for each of the ^{13}O, ^{10}C, and ^{15}O/^{17}Ne data sets are shown in Fig. 2. Peaks identified in these spectra are labeled by letters and the spins and parities we assigned to them (Secs. IV and V) are listed in Table I. A ^{10}C level scheme from this work is shown in Fig. 3 where, for comparison, the energies of the intermediate states are also shown.

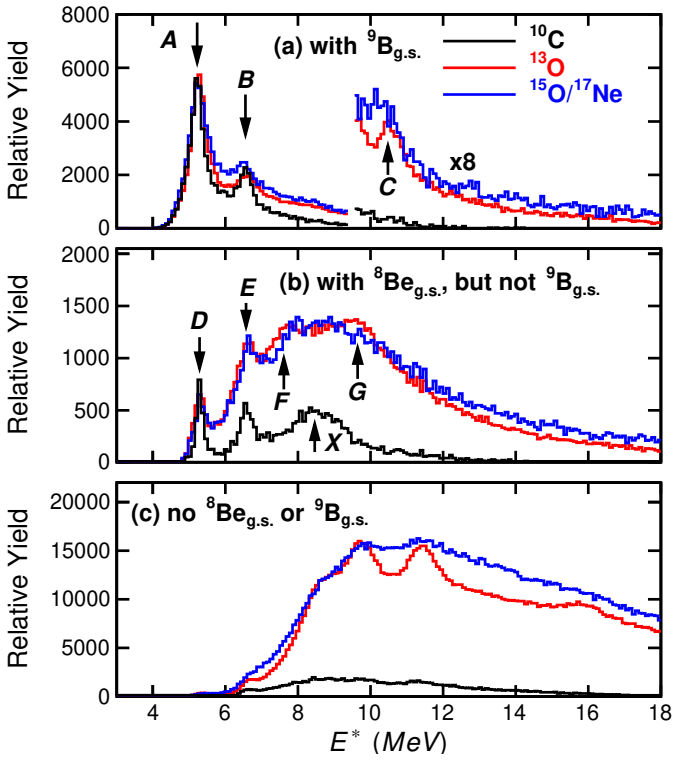

FIG. 2. Distributions of ^{10}C excitation energy obtain from $2p$+2α events, with the invariant-mass method, from three data sets studied in this work. (a) is for events which decayed through a $^{9}B_{g.s.}$ intermediate state, (b) is for events which decayed through an $^{8}Be_{g.s.}$ intermediate state, but not a $^{9}B_{g.s.}$ state, and (c) is for the remaining events. Peaks discussed in this work are labeled by letters. The results from each data set have been normalized so that the 2_2^+ peaks in (a) have the same maximum value.

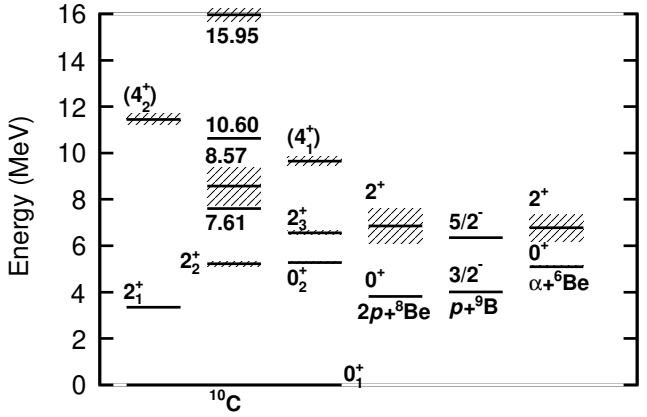

FIG. 3. Level scheme for ^{10}C showing the levels discussed in this work and their energies relative to the intermediate states. The levels are labeled by their spin, or if that is unknown, by their excitation energy in MeV.

For the events decaying through a $^{9}B_{g.s.}$ intermediate state [Fig. 2(a)], the invariant-mass spectra are all dominated by peak A at 5.222 MeV associated with the 2_2^+ excited state [30]. We have normalized the spectra from each data set to give a similar yield for this peak. Peak B is also present for each the three data sets. Finally, the ^{13}O and ^{15}O/^{17}Ne data sets show evidence of a higher-energy peak (C) at 10.6 MeV. Possibly this is same as the 10.48-MeV peak identified in the proton pickup reaction with a ^{9}C beam [13], but where the decay path was not determined.

Figure 2(b) shows the invariant-mass distributions for events which decay through an $^{8}Be_{g.s.}$ intermediate state, but are not fed by the decay of $^{9}B_{g.s.}$. Peaks D and E are prominent in the spectra from all three data sets and are associated with prompt $2p$ decays. The lower of these two peaks is identified as the J^π=0_2^+ state and is discussed in Sec. IV A. Peak X in the ^{10}C data set is not associated with a ^{10}C excited state and was attributed to target contamination in Ref. [15]. Also of interest are two other less prominent peaks, F and G, which are only observed in the ^{13}O data set and are best seen in Fig. 4(b) where the spectrum from this data set is shown by itself.

The third category of events, those that do not decay through an $^{8}Be_{g.s.}$ intermediate state [Fig. 2(c)], show evidence of additional peaks which are most pronounced in the ^{13}O data set. This category of events contains a number of possibilities including α decay to $^{6}Be_{g.s.}$ (Γ=92 keV), proton decay to the $5/2^-$ (E^*=2.345 MeV, Γ=81 keV) state of ^{9}B [which has a negligible branching ratio (0.5%) through $^{8}B_{g.s.}$], and decay paths involving much wider intermediate states. Contribution from wider intermediate states are very difficult to isolate, but the first two possibilities can be explored with an alternative gating scheme which, while it cannot separate these decays on an event-by-event basis, can give their excitation spectra.

In this scheme, the third category of events are subdivided into bins of ^{10}C excitation energy and the ^{9}B and ^{6}Be excitation-energy distributions from the invariant-mass of p+2α and $2p$+α subevents are constructed. For example, Fig. 5 shows the ^{9}B excitation-energy distributions from three -MeV-wide gates on the ^{10}C excitation energy centered at 7.75, 8.89 and 12.75 MeV. The $5/2^-$ state of ^{9}B at E^*=2.345 MeV is clearly visible in all spectra where its width is dominated by the experimental resolution. Such distributions are fit (solid curves) with a Gaussian peak plus a smooth polynomial background (dashed curves). The integrated peak values are then used to construct point-by-point the ^{10}C excitation spectra consistent with decays through $^{6}Be_{g.s.}$ and $^{9}B_{5/2^-}$. With the high-statistics ^{13}O data set, this procedure was performed with narrow 200-keV-wide gates of the ^{10}C excitation energy. The resulting spectra are shown Fig. 4(c) and 4(d) where a number of peaks are visible. After removing these last two contributions, the residual excitation spectrum for which no decay path has been determined is shown in Fig. 4(e) and it too displays a number of peaks.

TABLE I. Level parameters obtained from the fits to the $2p$+2α invariant-mass spectra of Figs. 4 and 6. A number of peaks observed in different exit channels at the same energy have been treated as decay branches of common parent states. The extracted branching ratios (BR) are listed but, except for the 2_3^+ state, these have not been corrected for detector efficiency. Spin assignments, when made, are also listed. The uncertainties listed are statistical, in addition there is a systematic uncertainty of 10 keV in the centroids [9, 24].

J^π	E^* [MeV]	Γ [keV]	peak	branch	BR	Data sets
2_2^+	5.222(4)	250(46)	*A*	p+^{9}B$_{g.s.}$		^{10}C, ^{13}O, ^{15}O/^{17}Ne
0_2^+	5.282(5)	96(57)	*D*	$2p$+^{8}Be$_{g.s.}$	>30%	^{10}C, ^{13}O, ^{15}O/^{17}Ne
2_3^+	6.556(10)	177(75)	*B*	p+^{9}B$_{g.s.}$	66(2)%	^{10}C, ^{13}O, ^{15}O/^{17}Ne
			E	$2p$+^{8}Be$_{g.s.}$	18(1)%	
			H	α+^{6}Be$_{g.s.}$	16(1) %	
	7.61(9)	<450	*F*	$2p$+^{8}Be$_{g.s.}$		^{13}O
1^+,$2^\pm$,$3^\pm$,4^+	8.57(2)	1645(40)	*L*	p+^{9}B$_{5/2^-}$		^{13}O, ^{15}O/^{17}Ne , ^{10}C(?)
(4_1^+)	9.647(21)	392(90)	*N*	other	46(2)% [a]	^{9}C, ^{13}O, ^{15}O/^{17}Ne
			I	α+^{6}Be$_{g.s.}$	27(2)% [a]	
			M	p+^{9}B$_{5/2^-}$	23(1)% [a]	
			G	$2p$+^{8}Be$_{g.s.}$	3.6(6)% [a]	
	10.603(23)	<230	*C*	p+^{9}B$_{g.s.}$		^{13}O, ^{15}O/^{17}Ne
(4_2^+)	11.450(9)	481(56)	*O*	other	86(1)% [a]	^{9}C, ^{13}O, ^{15}O/^{17}Ne
			J	α+^{6}Be$_{g.s.}$	9(1)% [a]	
				p+^{9}B$_{5/2^-}$	4.1(4)% [a]	
	15.953(24)	551(116)	*P*	other	88(2)% [a]	^{13}O
			K	α+^{6}Be$_{g.s.}$	12(2)% [a]	

[a] Branching ratios are not corrected for channel-dependent detector efficiencies.

Fits to invariant-mass spectra are shown in Figs. 4 and 6 as the solid red curves. These fits, and others presented in this work, include smooth background contributions (dashed-blue curves) associated with non-resonant contributions and wide unresolved resonances. As these backgrounds contributions cannot be presently calculated, our assumption is they represent the smooth behavior under the visible peaks. We fit the background using an inverse-Fermi function times a polynomial. The inverse Fermi function allows the fitted background to vanish as one decreases the decay energy towards the channel threshold. The polynomial is generally taken to be of first or second order. For narrow peaks sitting on small backgrounds, the choice of the background parametrization has little effect on the extracted peak parameters. The choice of background parametrization will be more important for wider peaks. For the very-wide peaks the differentiation between peak and background is not possible and the peak becomes part of the background.

For the resolved resonances in these figures we have assumed Breit-Wigner intrinsic line shapes with the experimental resolution and efficiency included via Monte Carlo simulations [24] except for a few cases where R-matrix intrinsic line shapes are utilized instead. The energy resolution of the detectors in the simulations have been fine tuned so as to reproduce the experimental line shapes of the ^{8}Be$_{g.s.}$, ^{9}B$_{g.s.}$, ^{9}B$_{5/2^-}$, and ^{6}Be$_{g.s.}$ intermediate states observed in the invariant-mass spectra of the subevents (Fig 1). At E^*=6.54 MeV, the FWHM of the simulated ^{10}C resolution is 252(38) keV and 340(20) keV for the low-energy ^{10}C inelastic scattering and higher-energy data sets, respectively.

The centroids and widths of the low-energy resonances have been largely determined from fits to the ^{10}C inelastic-scattering data set due to its superior energy resolution and peak-to-background ratios. Figure 6 shows such fits to peaks *A, B, D, E* and *H*. Peaks *B, E* and *H* has been assumed to be decay branches of the same state and so a single centroid and width were obtained from a joint fit to all the spectra in this figure. Originally we tried fitting these peaks with Breit-Wigner line shapes, but found some tension in fitting the width of peak *B* and the low-energy tail of peak *H* at the same time. This was resolved by using R-matrix lines shapes associated with the spin assignment of 2^+ (see Sec. IV D). The α-decay branch has the highest threshold and with an ℓ=2 centrifugal barrier, the barrier penetration factor rises rapidly in the vicinity of the peak giving this decay branch a skewed line shape. This allowed a better joint fit to the spectra and to the α+^{6}Be$_{g.s.}$ spectra from the ^{13}O data set with its much higher statistics [Fig. 6(d)]. More details of this R-matrix calculation can be found in Sec. V. Further evidence that peaks *B, E*, and *H* are branches of the same state is obtained from their fitted relative yields. Figure 7 shows the ratios of yields of peaks *B* and *H* relative to peak *E* obtained from the three data sets. These ratios are consistent between these data sets as expected for decay branches from a common state. While peaks *A* and *D* in the p+^{9}B$_{g.s.}$

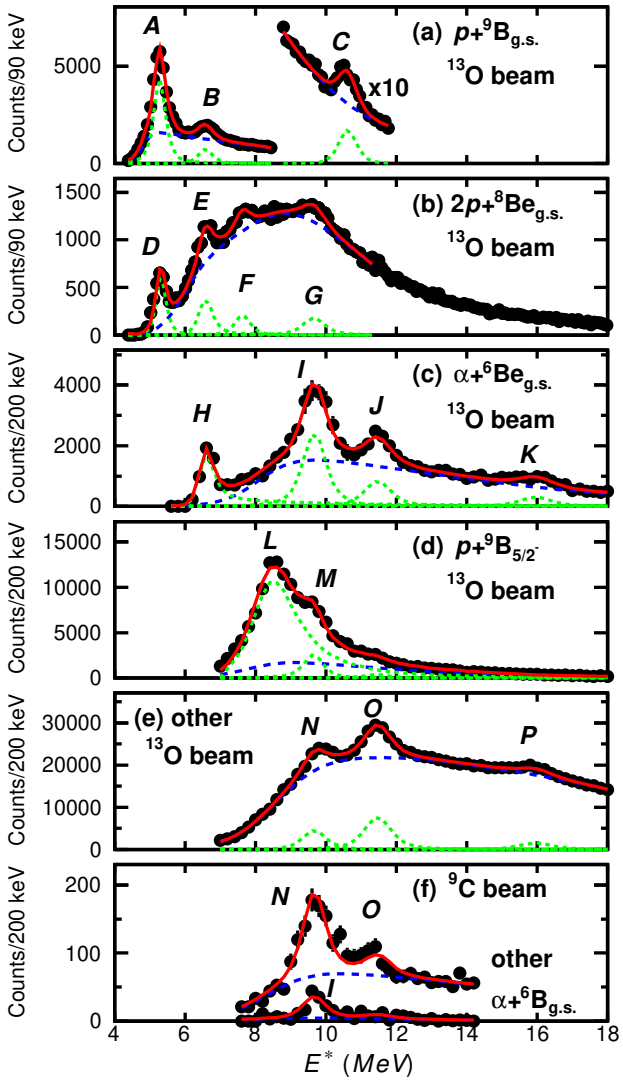

FIG. 4. (a-e) Distributions of ^{10}C excitation energy extracted from the ^{13}O data set for the specified decay paths. (f) distributions obtained with the ^{9}C data set. The solid-red curves show fits to these distributions with the dashed-blue curves showing the fitted background contributions and the dotted-green curves indicating the contribution from each of the resonances. Labels for the observed peaks are given.

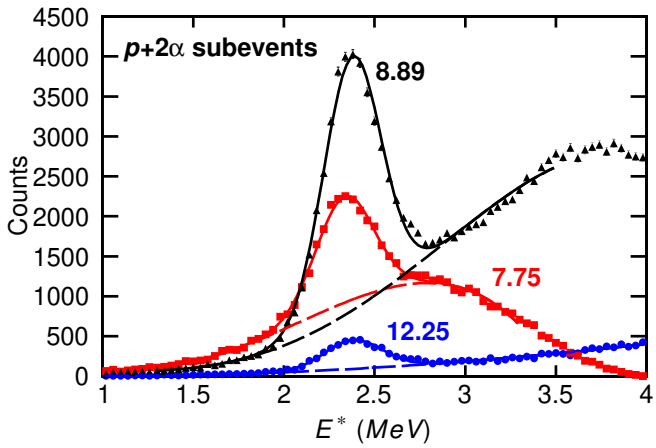

FIG. 5. Distributions of ^{9}B excitation energy from the invariant mass of p+2α subevents obtained from 2p+2α events with no ^{8}Be$_{g.s.}$ intermediate fragments and with a -MeV-wide gate on the ^{10}C excitation energy. The results here are from the ^{13}O data set and the distributions are labeled by the mean ^{10}C excitation energy of the gate. The solid curves are from fits with Gaussian peaks at the energy for the 5/2$^-$ state in ^{9}B plus smooth polynomial backgrounds (dashed curves).

and 2p+^{8}Be$_{g.s.}$ channels are separated by only ≈65 keV, their ratio of yields (Fig. 7) varies significantly in the three data sets indicating that these two peaks are associated with two different levels in ^{10}C.

For the other peaks, centroids and widths were constrained from fits to the high-statistics ^{13}O data set where these higher-energy peaks are most prominent. The fitted spectra are shown in Figs. 4(b) to 4(e). Peak L in Fig. 4(d) is very wide and a R-matrix intrinsic line shape for a single-channel was utilized. Unless an anonymously large channel radius is assumed, the wide width of this state cannot be reproduced with $\ell > 1$ giving the spin-parity possibilities listed in Table I. Again many of the peaks in the different channels fall at the same energy and so these were also treated as decay branches of common parent states and the level parameters were obtained from joint fits. Table I lists these decay branches and gives their fitted branching ratios. These have not been corrected for the detector efficiencies associated with the different decay branches as the momentum correlations between the decay products are not always known. The exception is for peaks B, D and H were the correlations can be estimated, i.e., peak B is treated as a series of sequential steps with ^{9}B$_{g.s.}$ and ^{8}Be$_{g.s.}$ intermediate states; peak E undergoes prompt 2p decay with the proton momenta sampling the correlations measured from the ^{10}C data set in Ref. [21]; and peak H α decays to ^{6}Be$_{g.s.}$, which then 2p decays sampling the momentum correlations measured in Ref. [7].

We note that the simulated efficiencies for these three channels are quite different with peaks B and E having efficiencies of 5 and 2.4 times smaller than calculated for peak H, respectively. This is a result of the strong correlations associated with the decay of ^{8}Be$_{g.s.}$ and ^{9}B$_{g.s.}$ intermediate states which have small decay energies and thus their decay fragments are emitted with small relative angles. Typically more than one of these decay fragments enter the same CsI(Tl) crystal and the event is not identified. Such strong correlations are not expected for the other decay channels identified in this work and the efficiencies, for the same parent state, are expected to be more similar. With this in mind, the uncorrected branching ratio of 3.6(6)% for peak G associated with 2p decay to the ^{8}Be$_{g.s.}$intermediate would be expected to increase significantly if the correction could be made.

Figure 8 compares the p+^{9}B$_{5/2-}$ spectrum obtained with the ^{13}O data set to those from the ^{10}C and ^{15}O/^{17}Ne data sets where the latter two spectra have been normalized to give the same maximum peak height. Due to

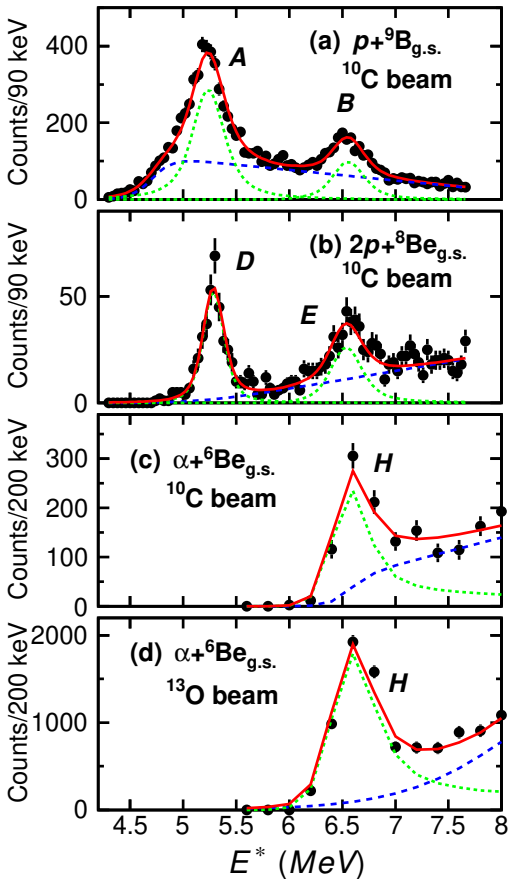

FIG. 6. (a-c) Distributions of ^{10}C excitation energy extracted from the ^{10}C data set for the specified decay paths. The lower-statistics α+^{6}Be$_{g.s.}$ distribution in (c) is compared to the higher-statistics version from the ^{13}O data set in (d). The solid-red curves show fits to these distributions with the dashed-blue curves showing the fitted background contributions and the dotted-green curves indicating the contribution from each of the resonances. Labels for each of the observed peaks are given. The fitted curves have the same binning in E^* as the experimental data.

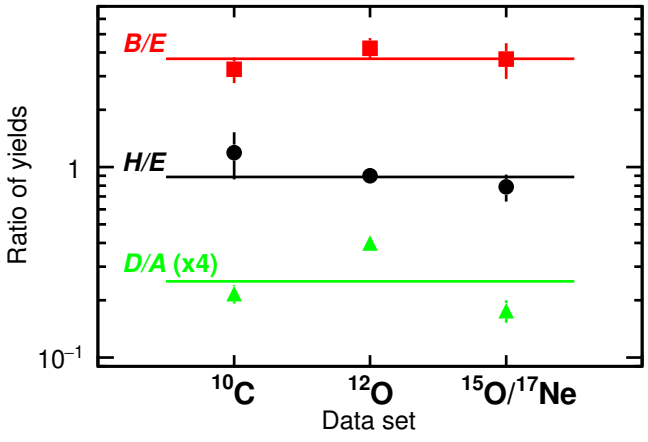

FIG. 7. Ratio of fitted yields of the specified peaks from the ^{10}C, ^{13}O, and ^{15}O/^{17}Ne data sets. The horizontal lines give the weighted mean ratios from all three data sets.

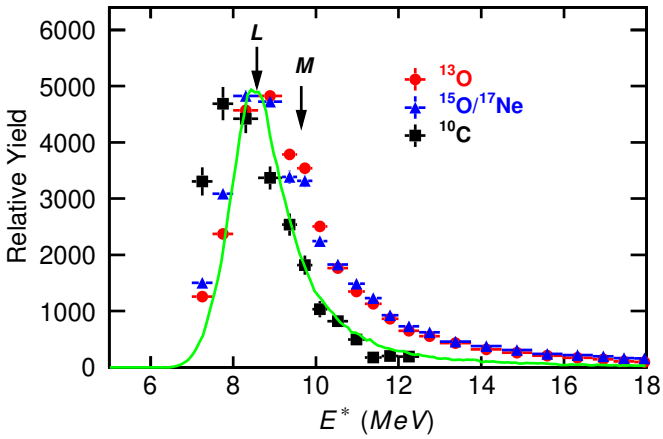

FIG. 8. Distribution of ^{10}C excitation energy for events which proton decay to the $5/2^-$ state in ^{9}B. Results are shown for three data sets considered in this work. The experimental data have been normalized to the same maximum value on the y axis. While the data for the ^{13}O and ^{15}O/^{17}Ne data sets can be fit with contributions from peaks L and M (see Fig. 4(d) for the ^{13}O data set), the ^{10}C data cannot. For comparison, the curve shows the fitted contribution from peak L obtained from the ^{13}O data set. The addition of contributions from peak M would not improve agreement with the ^{10}C data.

the lower statistics for the latter data sets, the spectra are now made with 400-keV-wide bins. The results for ^{15}O/^{17}Ne data have largely the same shape implying similar relative contributions from the two peaks, L and M. However, the result from the ^{10}C data set is quite different peaking at a lower energy. Even if the contribution from the higher-energy peak M is missing in the ^{10}C data set, the observed distribution still peaks lower in energy than the fitted line shape of peak L (green curve). This suggests that either there is another wide level associated with the p+^{9}B$_{5/2^-}$ channel or, more likely, the lower-energy inelastic-scattering reaction associated with the ^{10}C data set selectively populates the lower-energy part of the broad profile associated with resonance L.

A similar comparison between data sets is made for the α+^{6}Be$_{g.s.}$ channel in Fig. 9 where now the spectra are normalized to give the same height for peak I. Peak H is clearly resolved in all data sets and evidence for peaks I and J is also seen in all sets. Peak K, which has a very small peak-to-background ratio in the ^{13}O data set, is not visible in the other two sets.

For the ^{9}C data set where ^{10}C states are populated via neutron pickup reactions, peaks associated with ^{8}Be$_{g.s.}$ and ^{9}B$_{g.s.}$ intermediate states are relatively weakly populated [13]. This reaction is quite selective largely populating the 9.647-MeV state as seen in Fig. 4(f) where the two most intense branches N and I are observed. To a lesser extent, the 11.450-MeV state (peak O) is also observed. The peak-to-background ratio is much better for these states in this data set, but the statistics are smaller than the ^{13}O data set. The solid-red curves in Fig. 4(f) show fits to these spectra where the peak centroids and

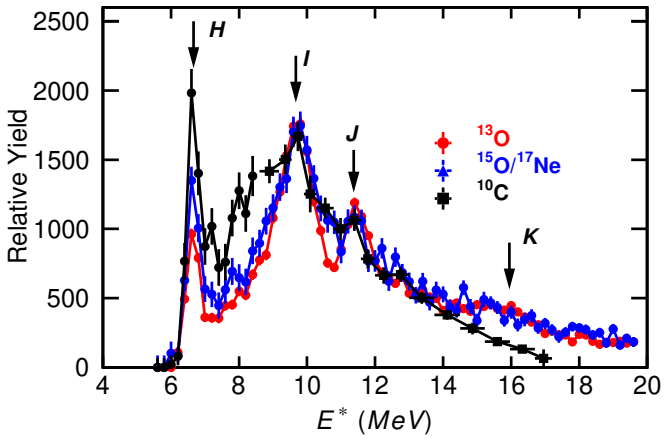

FIG. 9. Distribution of ^{10}C excitation energy for events which α decay to the ground state of ^{6}Be. Results are shown for three data sets considered in this work. The arrows indicate the location of fitted states tabulated in Table I. The results for each data set have been normalized to give the same peak maximum at 9.69 MeV.

widths are constrained to the fitted values obtained from the ^{13}O data set. The overall reproduction of these spectra are good.

III. ^{11}N STATES DECAYING TO THE $3p$+2α EXIT CHANNEL

In this section we will discuss ^{11}N states populating the $3p$+2α exit channel. Lower-energy states that populate the p+^{10}C channel from the ^{13}O data set have been presented in [9]. The ^{9,10}C and ^{15}O/^{17}Ne data sets have insufficient statistics for the $3p$+2α channel and will be ignored. As for the $2p$+2α events, the $3p$+2α events can be subdivided into the same three groups. As the ground-state of ^{11}N is not well constrained, we plot distributions of the total decay energy E_T instead. The spectrum associated with a ^{9}B$_{g.s.}$ intermediate state is plotted in Fig. 10(b) and four peaks (N, O, P and Q) are well resolved.

The solid-red curve shows a fit to this distribution with four Breit-Wigner intrinsic line shapes (dotted-green curves) and a smooth background (dashed-blue curves). Again, the experimental resolution and efficiency were included via Monte Carlo simulations [24]. The background shown in this figure was parametrizated as an inverse-Fermi function times a cubic polynomial in this figure and the fitted background has a rapid rise at around E_T ~2.5 MeV, possibility associated with an unresolved wider peak contributing along with the other background sources. However this background is not well defined under peaks O to Q which overlap. If instead, the background is parametrized with an inverse-Fermi function times a quadratic polynomial, the fitted background is found to be smaller and flatter and the fitted widths of peaks O to Q increased by factors from 1.5 to 3.

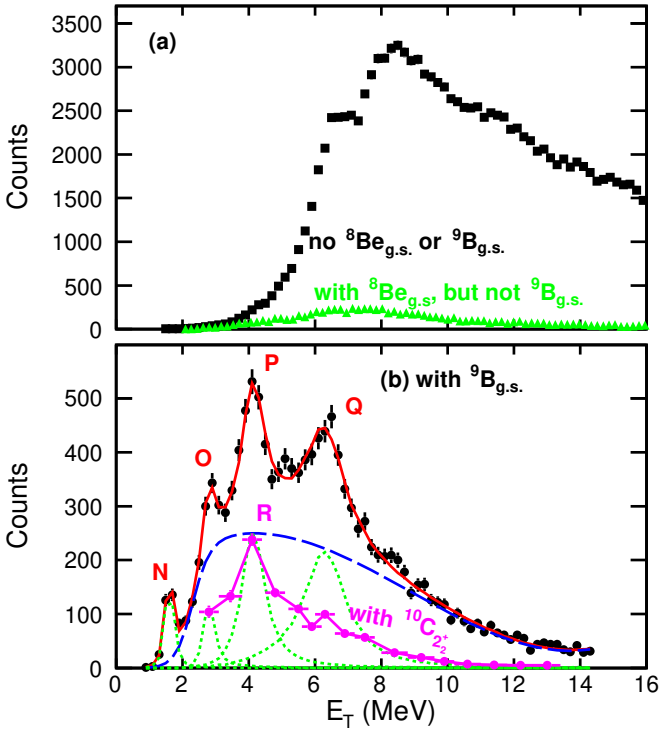

FIG. 10. Distributions of ^{11}N decay energy obtain from $3p$+2α events with the invariant-mass method. Events which are associated with a ^{9}B$_{g.s.}$ are shown in (b), while those with no ^{9}B$_{g.s.}$, either with or without an ^{8}Be$_{g.s.}$ are shown in (a). The solid-red curve in (b) shows a fit to this data with a background (dashed blue curve) and four peaks (dotted green curves). The magenta data points in (b) indicated the yield associated with proton decay to the ^{10}C$_{2_2^+}$ intermediate state. Labels for peaks discussed in this work are shown.

The fitted centroids are less sensitive to the background parametrization, with the largest change of 50 keV for peaks P and Q. The fitted parameters for peak N have also very little sensitivity to background parametrization as there is little background in its vicinity.

The fitted centroids and widths of the four peaks are listed in Table II where the uncertainty from the background parametrization is included. In addition the excitation energy based on the ground-state energy determined in [9] from the same data set is also listed. With these new states, the level scheme of ^{11}N is displayed in Fig. 11 where the first known decay steps are indicated by the arrows.

For the subdivision of events with an ^{8}Be$_{g.s.}$, but no ^{9}B$_{g.s.}$, intermediate state, the invariant-mass spectrum in Fig. 10(a) (green triangular data points) is rather featureless with no resolved states.

Similar to the analysis of the $2p$+2α events, those events without an ^{8}Be$_{g.s.}$ intermediate state can be analyzed to give the contributions from ^{9}B$_{5/2^-}$ and ^{6}Be$_{g.s.}$ intermediate states. The ^{11}N decay energy spectra for these events are plotted in Fig. 12. The result for the ^{6}Be$_{g.s.}$ intermediate state [Fig. 12(a)] shows no promi-

TABLE II. Level parameters obtained from the fits to the $3p$+2α invariant-mass spectra of Figs. 10(b) and 12. The intermediate states identified from the correlations are indicated. The excitation energy is based on the ground-state mass obtained from the same data in Ref. [9]. The uncertainties listed are statistical, in addition there is a systematic uncertainty of 10 keV in the centroids [9, 24].

J_π	E_T [MeV]	E^* [MeV]	Γ [keV]	peak	intermediate state
$3/2^-_2$	1.588(18)	3.940(18)	136(24)	N	$^9B_{g.s.}$
$(5/2^-)$	2.774(40)	5.126(40)	492(239)	O	$^9B_{g.s.}$
$(7/2^-)$	4.081(104)	6.433(104)	836(338)	P	$^9B_{g.s.}$
				R	$^{10}C_{2^+_2}$
$(9/2^-)$	6.390(70)	8.742(70)	1770(356)	Q	$^9B_{g.s.}$
	6.919(58)	9.271(58)	1126(201)	S	$^9B_{5/2^-}$
	8.695(67)	11.047(67)	1825(239)	T	$^9B_{5/2^-}$

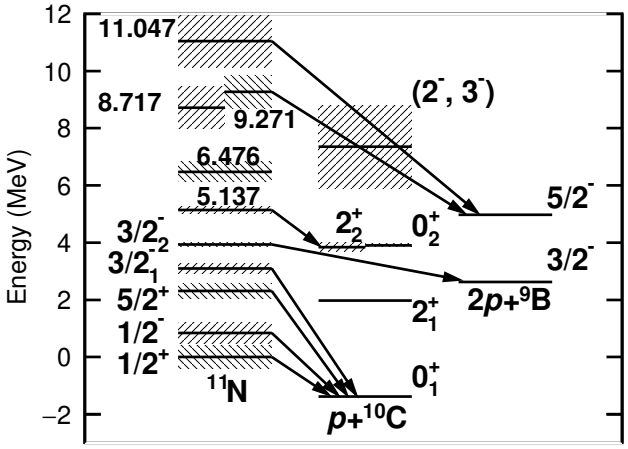

FIG. 11. Level scheme for ^{11}N states obtained in this work and from Ref. [9]. Where known, the first step in the decay of each level, either $1p$ or $2p$ emission, is indicated by an arrow.

nent peaks, while one can resolve two peaks in the results for the $^9B_{5/2^-}$ intermediate state [Fig. 12(b)]. The solid curves show a fit to this spectrum with three contributing R-matrix line shapes for diproton emission to $^9B_{5/2^-}$ [31]. Again the effect of the detector efficiency and resolution was included via Monte Carlo simulations. The higher-energy peak in the fit is not resolved in the experimental data and could in fact represent a background from multiple peaks and other sources. The two lower-energy peaks (S and T) are located at E_T=6.919(58) and 8.695(67) MeV with widths of 1.126(201) and 1.825(239) MeV, respectively.

Finally for the subdivision of events which decay through $^9B_{g.s.}$, we can use a similar scheme to look for ^{10}C intermediate states by projecting the E_T values for $2p$+2α subevents with gates on the ^{11}N invariant mass. Within the statistics, only the 2^+_2 excited state of ^{10}C could be identified. This intermediate state, of course, proton decays to the $^9B_{g.s.}$ state. The invariant-mass

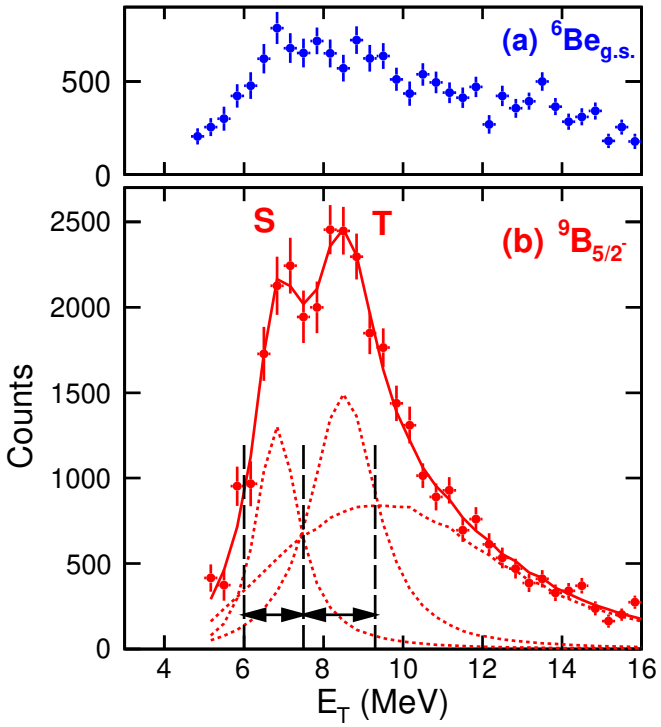

FIG. 12. Distributions of ^{11}N decay energy obtain from $3p$+2α events which contained (a) a $^6Be_{g.s.}$ or (b) a $^9B_{5/2^-}$ intermediate state. The $^9B_{5/2^-}$ results have been fit (solid curves) with the sum of three ^{11}N peaks (dotted curves) where the detector efficiency and resolution has been incorporated via Monte Carlo Simulations. Gates are indicated for which two-proton correlation plots are displayed in Fig. 16. Labels for the two peaks discussed in the text are given.

distribution associated with the $^{10}C_{2^+_2}$ state is shown by the magenta data points in Fig. 10(b) where one peak, labeled R is visible. This peak is at the same energy as peak P and thus represents one decay branch of a state at E_T=4.124 MeV. It is possible that peaks O, P and Q have branches from other ^{10}C intermediate states and there may also be yield associated with prompt $2p$ emission directly to $^9B_{g.s.}$. Peak N, the lowest-energy of the ^{11}N peaks, decays predominantly by prompt two-proton emission and is discussed in Sec. IV B.

IV. $2p$ DECAY

Before considering prompt $2p$ decay of excited states in ^{10}C and ^{11}N, let us briefly review prompt $2p$ decay from ground states. Ground-state $2p$ decay has been observed from a number of even-Z nuclides ranging from ^{6}Be to ^{67}Kr [32]. The lightest cases, ^{6}Be, ^{11,12}O and ^{15,16}Ne are associated with democratic $2p$ decay where there exists a wide intermediate state (the $Z-1$, $A-1$ ground state) [1]. The complete momentum correlations in $2p$ decay can be represented by a two-dimensional distribution [33] which has only been measured with high statistics for

three ground-state emitters, i.e. the democratic decays of ^{6}Be$_{g.s.}$ [7], ^{12}O$_{g.s.}$ [9], and ^{16}Ne$_{g.s.}$ [23]. The next best case is for ^{45}Fe where the correlations were extracted from 75 events [3, 34]. Theoretical studies show that the correlations are determined by the initial-state nuclear structure modified by the decay dynamics and final-state interactions [3, 7, 22, 33, 35].

Comparison of the correlations between different emitters is most easily made via their one-dimensional projections. In this work we consider projected distributions on the quantities E_{core-p}/E_T and E_{p-p}/E_T, where E_{core-p} is the relative energy between one of the protons and the core and E_{p-p} is the relative energy between the two protons. These are complementary variables and give information on different aspects of the system. For the former, there are two possible values for each $2p$ decay and both are used to increment the presented distributions.

A comparison of the projected correlations for ^{6}Be$_{g.s.}$, ^{12}O$_{g.s.}$, and ^{16}Ne$_{g.s.}$ obtained from Refs. [7, 9, 23] is shown in Fig. 13 where these distributions are indicated by the dotted curves and are normalized to the same total yield. These decays are from 0^+ initial states to 0^+ final states and hence the two protons remove no net angular momentum. In addition, these $2p$ emitters have quite similar decay energies Q_{2p}=1.37-1.72 MeV which are listed individually in the figure. The correlations for ^{12}O and ^{16}Ne are almost identical and the E_{p-p}/E_T distribution for ^{6}Be is not very different from those of the heavier $2p$ emitters.

Prompt emission of two protons from the same single-particle orbital is expected to be characterized by $E_{core-p}/E_T \approx 0.5$, i.e. the two proton are emitted with similar kinetic energies as this maximizes the product of their barrier penetration factors for a fixed total decay energy. This feature is demonstrated in Fig. 13(b) in all the experimental distributions. The distribution for ^{6}Be is wider than the two heavier ground-state emitters. As the charge of the α core in ^{6}Be is small, the Coulomb focusing to $E_{core-p}/E_T \approx 0.5$ is not as strong in this case. In addition as the core is also very light, recoil effects will be larger for ^{6}Be. The E_{p-p}/E_T quantity is closely related to the relative angle between the emitted protons, with small relative energies and angles often called di-proton-like and large values associated with back-to-back proton emissions sometimes referred to as cigar configurations.

Different single-particle configurations of the two valence protons give rise to different relative-angle distributions inside the nucleus. For instance, $[s_{1/2}]^2_{J=0}$ and $[p_{1/2}]^2_{J=0}$ configurations have isotropic distributions, while $[p_{3/2}]^2_{J=0}$ configurations have significant di-proton and cigar correlations. In principle there can be more than one configuration which would make the relative angle distributions more complex due to interference effects. In Ref. [9] it was argued that the similarity of the E_{p-p}/E_T distributions for ^{12}O and ^{16}Ne emitters is due to the fact that these decays are dominated by the $[1s_{1/2}]^2_{J=0}$ component. For instance, with an initial wavefunction of ^{12}O with 36% $[s_{1/2}]^2_{J=0}$, 25% $[0p_{1/2}]^2_{J=0}$, and 14% $[0d_{5/2}]^2_{J=0}$ [5], a time-dependent calculation of its decay by Wang and Nazarewicz showed that the $[s_{1/2}]^2_{J=0}$ component accounted for 73% of the emitted proton pairs [35]. The initial wavefunction of ^{16}Ne is also expected to have a significant $[1s_{1/2}]^2_{J=0}$ component with predictions of 45(5)% [36] and 50-75% [37] with most of the remaining strength being $[0d]^2_{J=0}$. As the decay of the latter is greatly suppressed by barrier penetration, the ^{16}Ne decay should also be dominated by $[1s_{1/2}]^2_{J=0}$ emission.

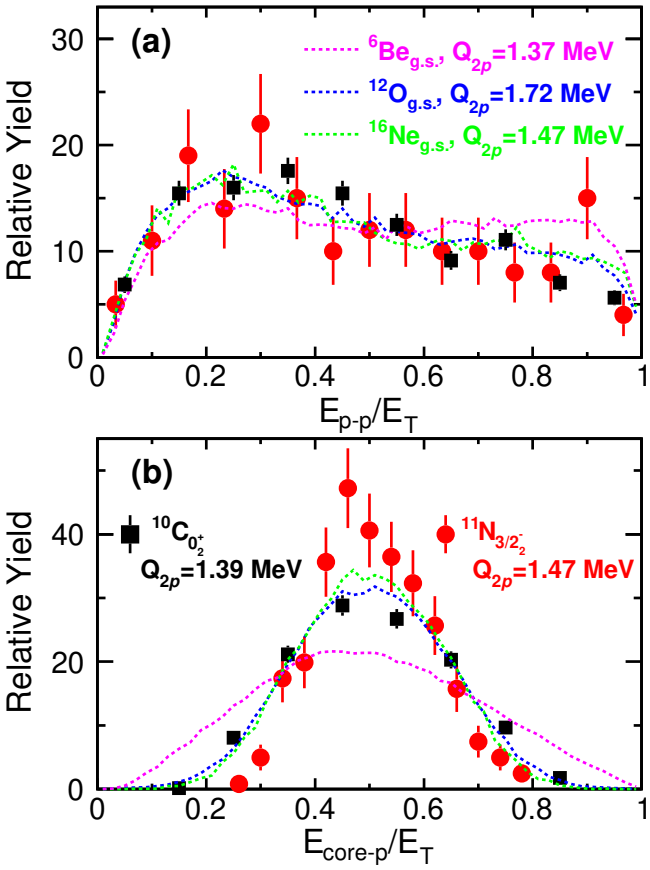

FIG. 13. Correlations plots (data points) for the two-proton decay of the ^{11}N$_{3/2_2^-}$ (red) and ^{10}C$_{0_2^+}$ (black) states. (a) shows the relative p-p energy while (b) shows the p-core relative energy. For comparison, experimental results from the ground-state two proton decay of ^{6}Be, ^{12}O, and ^{16}Ne are displayed as the dotted curves. Each data set was normalized to give the same integrated yield.

Unlike the ^{12}O and ^{16}Ne nuclides, the internal wavefunction for ^{6}Be is not expected to have significant $[1s_{1/2}]^2_{J=0}$ strength, but should be dominated by the $[0p_{3/2}]^2_{J=0}$ component instead. However, theoretical calculations indicate that this component mixes with the $[1s_{1/2}]^2_{J=0}$ configuration during the barrier penetration phase [22, 33, 35]. The final observed distribution is predicted to have roughly equal contributions from both $[0p_{3/2}]^2_{J=0}$ and $[1s_{1/2}]^2_{J=0}$ configurations which explains its similarity to the $[1s_{1/2}]^2_{J=0}$ dominated E_{p-p}/E_T dis-

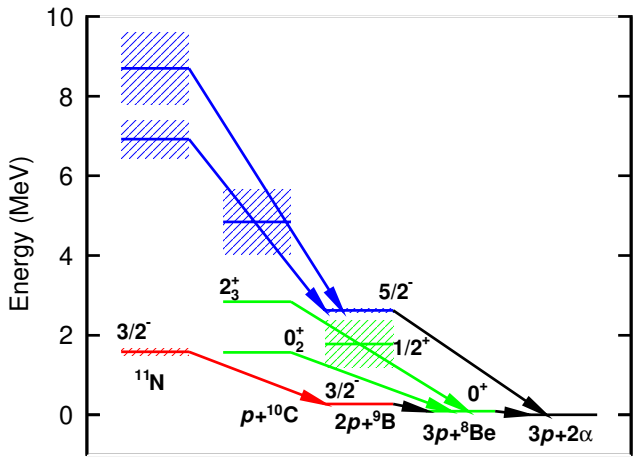

FIG. 14. Level diagram showing the states in ^{11}N and ^{10}C associated which $2p$ decay and states of interest in their decay. For each $2p$ emitter, the initial, wide intermediate state, and $2p$-residual states are shown in the same color.

tributions for ^{12}O and ^{16}Ne. The most significant difference in the E_{p-p}/E_T distributions between ^{6}Be and the heavier emitters is in the region near back-to-back emissions, where the $[0p_{3/2}]^2_{J=0}$ component is relatively stronger in the former. These measured correlations can serve as templates to identify $2p$ emission with no net angular momentum removal in light nuclei located in the p and sd shells, though care should be taken for much smaller or larger decay energies. For heavier systems we note that the E_{p-p}/E_T distribution for ^{45}Fe in Ref. [3, 34] is much different to those in Fig. 13 as very little $[1s_{1/2}]^2_{J=0}$ component [38] is expected.

A. 0^+_2 state of ^{10}C

Fortune and Sheer predict the second 0^+ state in ^{10}C has a configuration of an ^{8}Be core coupled to two protons in the sd shell and its decay via p-wave emissions is very small [39]. In particular, their calculations indicate it has a large $[s_{1/2}]^2_{J=0}$ component and thus we may observe its $2p$ decay to ^{8}Be. This decay would be democratic as there exists a wide intermediate state, the $1/2^+$ first excited state of ^{9}B, which is expected to be an s-wave resonance. See Fig. 14 for the energy of this state relative to the initial and final states. We have used the ENSDF values for the ^{9}B$_{1/2^+}$ state [30] in this plot, but note that its energy and width are not well determined [40].

The two-dimensional momentum correlations between the three decay fragments in the $2p$ decay of ^{10}C to ^{8}Be$_{g.s.}$ for peaks D and E were presented from the ^{10}C data set in Ref. [15]. We will first concentrate on the peak D which was tentatively assigned as the 0^+_2 state in that reference. The correlations for peak E will be discussed later. The ^{10}C data set is preferred for these correlations as, while the counting statistics are not the largest, the peak-to-background ratio and invariant-mass resolution are the best of all the data sets.

Since the original measurement of these ^{10}C correlations, momentum correlations associated with the democratic $2p$ decay of ^{6}Be [7], ^{12}O [26], and ^{16}Ne [23] 0^+ ground states to 0^+ residual states have been measured and we now compare these to the ^{10}C* correlations in Fig. 13 where the results for the peak D are shown by black-square data points. This is a useful comparison as the $2p$ decay energy of this state to ^{8}Be is Q_{2p}=1.466(50) MeV which is comparable to those for the ground-state emitters which are listed in the figure. As expected for $2p$ decay, the E_{core-p}/E_T distribution is peaked at 0.5. More importantly, the correlations are almost identical to the ^{12}O$_{g.s.}$ and ^{16}Ne$_{g.s.}$ results which are dominated by $[1s_{1/2}]^2_{J=0}$ emission. This suggests that the decay of this ^{10}C state also has a substantial $[1s_{1/2}]^2_{J=0}$ component which fixes its spin as 0^+.

The E_{p-p}/E_T distribution for this ^{10}C state is closer to the ^{12}O and ^{16}Ne results than the ^{6}Be data and thus we conclude that the $[1s_{1/2}]^2_{J=0}$ component is likely associated with the initial wavefunction and not due to the effect of the decay dynamics as in ^{6}Be. With a significant $[1s_{1/2}]^2_{J=0}$ component, we expect to see a sizable Thomas-Ehrman shift between the energy of this level and its analog in ^{10}Be. The levels of the mirror pair are compared in Fig. 15 and indeed both the 0^+_2 and 2^+_2 levels have Thomas-Ehrman shifts. The latter is probably due to a $[1s_{1/2}, 0d_{5/2}]_{J=2}$ configuration. For the 0^+_2 state, Fortune and Sherr predict a Thomas-Ehrman shift of 1.00(11) MeV [39] which is very close to the value of 0.892(15) MeV obtained in this work.

The partial width for p-wave decay to ^{9}B$_{g.s.}$ is predicted to be very small (4^{+4}_{-2} keV) by Fortune and Sherr [39]. Experimentally such a decay branch would lie in our first subdivision of the $2p$+2α events and should be found in the invariant-mass distributions of Fig. 2(a). We see no evidence of such a branch, but our sensitivity is reduced as, at this energy, the invariant-mass spectra are dominated by the peaks associated with the more intense 2^+_2 state (peak A). We place a 70% upper limit on this p+^{9}B$_{g.s.}$ branching ratio at the 2σ level by fitting the spectra in Fig. 2(a) with an extra peak of the same energy and width as peak D in addition to observed peaks.

B. $3/2^-_2$ state of ^{11}N

Fortune has predicted an excited $3/2^-$ state in ^{11}N with two protons in the sd shell coupled to a ^{9}B$_{g.s.}$ core [41]. The predicted partial decay widths for p-wave emissions to the ground and first excited states in ^{10}C were small and so we also consider whether this state will decay to ^{9}B$_{g.s.}$ via $2p$ emission. The candidate for this state is peak N, the lowest of the resolved states in Fig. 10(b). The fitted width for this state of 136(24) keV makes it the narrowest ^{11}N state known.

Its momentum correlations (red data points) are compared to the ground-state systematics in Fig. 13. We again note that its $2p$ decay energy of

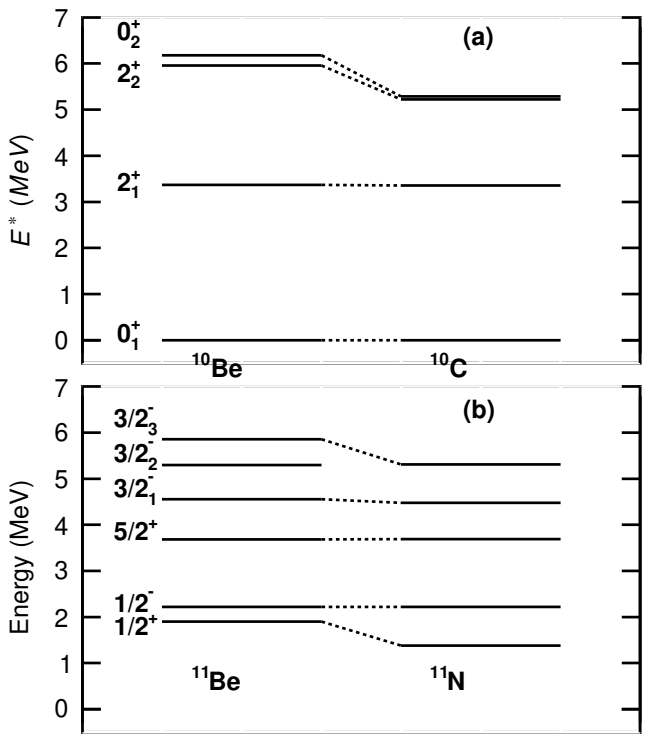

FIG. 15. Level schemes for the mirror pairs (a) ^{10}Be-^{10}C and (b) ^{11}Be-^{11}N showing the Thomas-Ehrman shifts for the second 0^+ state in (a) and the second $3/2^-$ state in (b). The energies of the levels in ^{11}N are given relative to the p+^{10}C threshold, whereas for ^{11}Be we have shifted them so that $1/2^-$ state lines up with its analog in ^{11}N.

Q_{2p}=1.303(12) MeV is comparable to the values for the ground-state systematics and that the E_{p-core}/E_T distribution is peaked near 0.5 as expected for $2p$ decay. Its correlations are also very similar to the $^{12}O_{g.s.}$ and $^{16}Ne_{g.s.}$ results indicating a significant $[1s_{1/2}]^2_{J=0}$ decay component and thus its spin is $3/2^-$. The statistical error bars are larger in this case and it is possible that the E_{p-p}/E_T distribution is consistent with the ^{6}Be result where the $[1s_{1/2}]^2_{J=0}$ component is a result of the decay dynamics rather than the initial wavefunction.

However, if the initial wave function has a significant $[1s_{1/2}]^2_{J=0}$ component, then we would expect to see a Thomas-Ehrman shift relative to its analog in ^{11}Be. Care must be taken in accessing the magnitude of the Thomas-Ehrman shift as the $1/2^+$ ground state of ^{11}N is expected to be an s-wave resonance [42] and a consistent centroid has not been found in experimental studies. In Fig. 15(b), the known levels as listed in [9], plus the results of this work, are plotted at their energy above the p+^{10}C threshold. The analog levels in the mirror nucleus ^{11}Be from the ENSDF data base [30] have been shifted so that the $1/2^-$ first excited states line up. With this shift, the second and third excited states also approximately line up and the ground states shows a significant Thomas-Ehrman shift as expected. The ENSDF data base lists three $3/2^-$ states in ^{11}Be within an interval of 1.5 MeV as seen in Fig. 15(b). This leaves the question as to whether our second observed $3/2^-$ in ^{11}N is the analog of the second or third $3/2^-$ ^{11}Be level in the ENSDF data base. However, we note that some studies suggest that the second-listed $3/2^-$ state is actually J^π=$3/2^+$ [43, 44]. Fortune has identified the third listed $3/2^-$ state in ^{11}Be as the one with large sd configuration strength [41]. With this assignment, we find a Thomas-Ehrman shift of 0.542(12) MeV which is 62% of the shift measured for the 0_2^+ state of ^{10}C and implies a smaller $[1s_{1/2}]^2_{J=0}$ component.

Relative to this same reference state, Fortune's predictions imply a Thomas-Ehrman shift of 1.07 MeV. This predicted shift is associate with a $[1s_{1/2}]^2_{J=0}$ component with a strength of 84%. However, Fortune notes that alternatively a $[1s_{1/2}, 1d_{5/2}]_{J=2}$ component could give to rise a similar shift. In any case, the predicted shift is too large and also points to the delicate balance involved in terms of the amount of $[1s_{1/2}]^2_{J=0}$ component. One might expect that by increasing this component it increases the $2p$ decay probability, but in the work of Fortune this results in a large Thomas-Ehrman shift which reduces the $2p$ decay energy to 0.78 MeV, significantly less than the experimental value of 1.303(12). The penetration factor for the emission of two protons changes rapidly with decay energy and a change of this magnitude would greatly suppress $2p$ emission.

The magnitude of this suppression depends on the competing decay branches. Fortune indicates that single-proton p-wave decay to the 2_1^+ first excited state of ^{10}C should dominate these competing branches with a partial width of ≈70 keV. The total width, extracted from the fitting of the invariant-mass spectra, is 136(4) keV suggesting a $2p$ decay width of ≈60 keV with two decay branches of similar magnitude. This $1p$ decay branch should populate the p+^{10}C invariant-mass spectrum at E_T=1.957(12) MeV after removing the energy of the γ-ray which de-excites the 2_1^+ state in ^{10}C. This spectrum is shown in Fig. 4(b) in [9], but unfortunately the contribution from this decay branch lies under the peak associated with the $1/2^-$ first excited state of ^{11}N which dominates the spectrum. Thus we are not very sensitive to this decay branch. Fits to the p+^{10}C invariant-mass spectrum, when adding an extra peak for this state, gives a maximum limit to the $1p$ branching ratio to the 2_1^+ state of 40% at the 2σ level which is close to Fortune's estimate.

If we consider the $2p$ decay of this ^{11}N excited state as a democratic $2p$ decay, like the 0_2^+ state of ^{10}C and the ground states of ^{6}Be, ^{12}O, and ^{16}Ne, then there should exist a wide intermediate state in ^{10}C. No such state is known experimentally. If like in these democratic $2p$ emitters the intermediate state is an s-wave resonance, then its spin would be 1^- or 2^-. States of this spin exist in the mirror nucleus ^{10}Be at the appropriate excitation energies, but their analogs in ^{10}C have yet to be identified.

C. Peaks S and T in ^{11}N

Peaks S and T located at E^*=9.271 and 11.047 MeV (E_T=6.919 and 8.695 MeV) were found to decay though the $5/2^-$ state in ^{9}B must be considered as a democratic $2p$ emitters. The only possible intermediate state in ^{10}C that decays through ^{9}B$_{5/2^-}$ is the wide peak L at E^*=8.4 MeV which is an s or p-wave resonance. Figure 14 shows the location of this intermediate state relative to the initial ^{11}N states and the $5/2^-$ state in ^{9}B.

The correlations for these states are compared to the ^{12}O and ^{6}Be ground-state results in Fig. 16. The experimental correlations were determined for the gates on E_T shown in Fig. 12(b) and from the fit we can see that they are not entirely clean as these states overlap and there is significant background under the fitted peaks. The E_{core-p}/E_T distributions are peaked near 0.5 as expected for prompt $2p$ emission and surprisingly, the correlations are almost identical to each other and to those obtained for ^{12}O$_{g.s.}$ which might suggest that they are dominated by $[1s_{1/2}]^2_{J=0}$ emission. However one should be very cautious here, the $2p$ decay energy for these two states are Q_{2p}=4.235(49) and 6.011(68) MeV, respectively, much greater than the value of Q_{2p}=1.718(15) for ^{12}O, so if there is a strong Q_{2p} dependence on the $[1s_{1/2}]^2_{J=0}$ correlation, this comparison will be misleading. Further work is needed to understand the structure of these states.

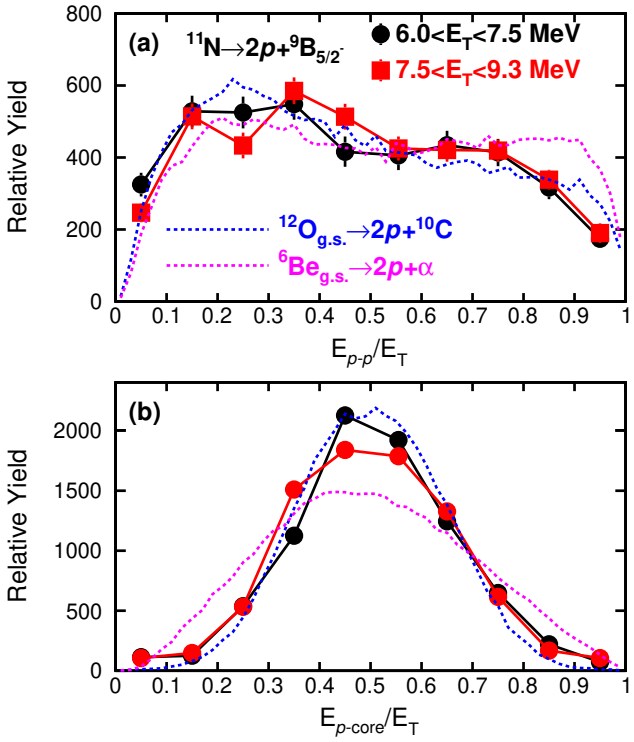

FIG. 16. Correlations plots (data points) for the two-proton decay of ^{11}N states to a ^{9}B$_{5/2^-}$ residual. Results are shown for the two gates indicated in Fig. 12 centered around the fitted ^{11}N peaks. These results are compared to correlations associated with two-proton decay from the ground states of ^{12}O and ^{6}Be from Refs. [7, 26]. Each data set was normalized to give the same integrated yield.

D. 2^+_3 state in ^{10}C

A second state in ^{10}C which $2p$ decays to ^{8}Be$_{g.s.}$ is peak E. Its correlations, shown as the data points in Fig. 17, are different to the other momentum correlations considered so far as there is a strong enhancement of small E_{p-p} values, i.e. diproton-like emissions. Similar enhancement has been observed in $2^+\rightarrow0^+$ $2p$ decays as shown in Fig. 17 which compares the ^{10}C correlations to known J^π=2^+ $2p$ emitters in ^{6}Be, ^{12}O, and ^{16}Ne [7–9]. The E_{p-core}/E_T distributions show an evolution from a single peak centered at 0.5 typical of ground-state $2p$ emitters to bi-modal distributions one would expect to find in sequential-decay scenarios. However, the E_{p-p}/E_T distributions are not consistent with sequential decay and show little variation among the different 2^+ states with strong diproton-like peaks similar to that found for peak E in ^{10}C. This enhancement of the diproton-like decay can be considered as a fingerprint for $2^+\rightarrow0^+$ decays, at least in this mass region. However theoretical studies are needed to understand the preference for diproton-like emissions and the evolution of the E_{p-core} distributions. From the comparison in Fig. 17 we associated peak E with the $2p$ decay of a 2^+ state in ^{10}C, the third-known 2^+ state in this isotope. This state also has α and $1p$ decay branches (Table I).

V. DISCUSSION

The cores of the $2p$ emitters investigated in this work, ^{8}Be$_{g.s.}$, ^{9}B$_{g.s.}$ and ^{9}B$_{5/2^-}$ all have strong α-cluster structure. The ^{9}B$_{5/2^-}$ state is often considered as the second member of the K^π=$3/2^-$ ground-state rotational band. Additionally, the analog of the 0^+_2 state in ^{10}Be is considered a cluster state, the band head of a rotational band [45, 46] with the two valence neutrons located in σ molecular orbits. Similarly, the analog of the $3/2^-$ state in ^{11}Be has been tentatively assigned as a cluster state, the band head of a K^π=$3/2^-$ rotational band [17, 47, 48]. Thus the extent of α clustering in the observed ^{10}C and ^{11}N states should be considered.

A. α-cluster states in ^{10}C

Figure 18 compares both ground-state and 0^+_2 rotational bands in the mirror nuclei ^{10}Be and ^{10}C where we have added spin assignments to some of the states discussed in this work. The α-cluster states in ^{10}Be were identified in Refs. [19, 49, 50]. For the second member of the 0^+_2 band in ^{10}C, we have assigned the 2^+_3 excited state associated with peaks B, E and H. Like the 0^+_2

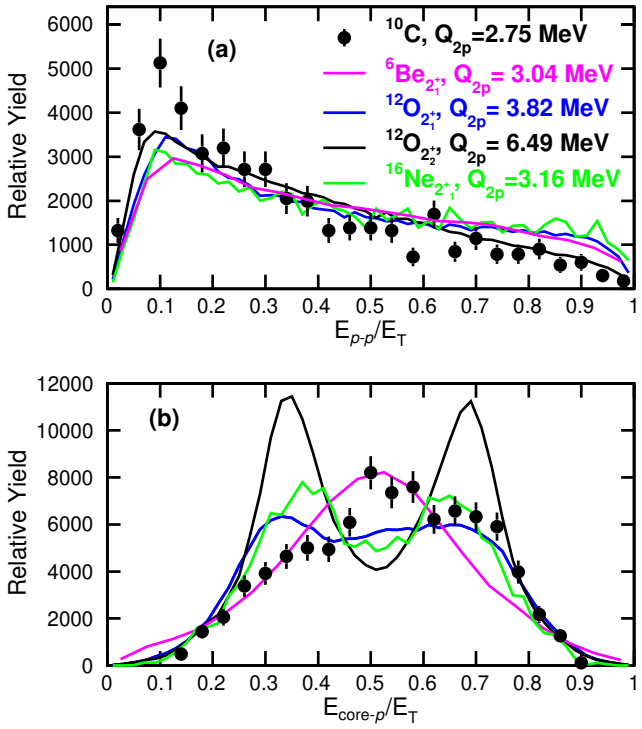

FIG. 17. Correlations plots (data points) for the two-proton decay of peak E obtained from the ^{10}C data set. These correlations are compared to experimental two-proton correlations from known 2^+ states from Ref. [7–9] shown by the solid curves. The $2p$ decay energies for each state are listed.

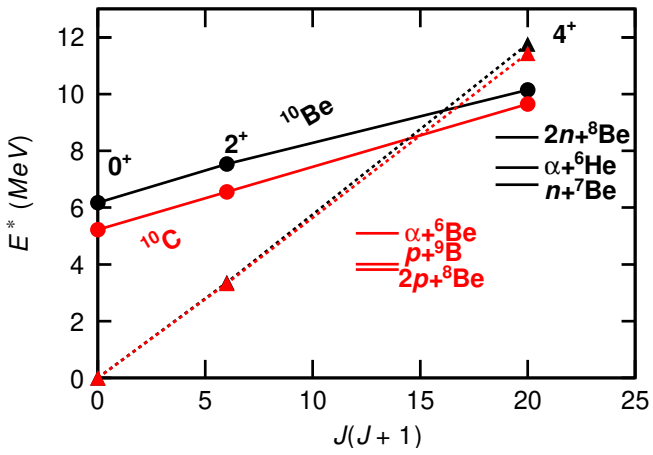

FIG. 18. Spin dependence of rotational bands in the mirror nuclei ^{10}Be (black) and ^{10}C (red). The levels for ^{10}Be are taken from Ref. [19, 49, 50]. The levels for the excited band in ^{10}C and the 4^+ member of the ground-state band are assigned from this work. Thresholds are shown for the decay channels of interest in both mirror nuclei. The dotted and solid lines connect the data points from the ground-state and excited 0^+ bands, respectively.

band head, this state also has a $2p$ decay branch. In addition as this state is above the α-decay threshold, we see the significant α decay branch expected for an α-cluster structure. The slope of the rotation curve between the assigned 0^+ and 2^+ states in Fig. 18 is similar to that for the mirror, suggesting they have very similar moments of inertia. The next J^π=4^+ member of this rotational band is tentatively assigned to the 9.647-MeV state associated with peaks *N, I, M,* and *G*. Like its lower 2^+ member, this state has $2p$ and α decay branches. However the strongest decay branch listed in Table I is "other", i.e. unknown. With the larger spin, we would expect both $2p$ and α decays to the 2^+ excited states in ^{8}Be and ^{6}Be to contribute to this "other" category. However these intermediate states are wide making it impossible to separate these decay branches and isolate them from other possible decay paths. The choice of this state for the 4^+ member also maintains the same slope of the rotational curve in Fig. 18 consistent with the ^{10}Be counterpart.

The 2^+ second member of the ground-state rotational band is the well-known first excited state of ^{10}C at E^*=3.353 MeV [30]. The 4^+ member of the mirror ^{10}Be ground-state rotational band is plotted as the 11.76 MeV state following the suggestion of Hamada *et al.* [49]. Our 11.450 MeV state is a good candidate for its analog in ^{10}C. It is interesting that our two assigned 4^+ states are the levels which are selectively excited in the neutron pickup reactions associated with the ^{9}C data set [Fig. 4(f)]. Transfer of nucleons to low-ℓ orbitals is suppressed for fast beams due to energy and momentum mismatch [51]. To produce 4^+ states, the neutrons must be transferred to ℓ=3 or 5 single-particle orbits, which are relatively high ℓ for such a light nucleus. This helps ameliorate the suppression due to the energy and momentum mismatch. However these states must still have some non-negligible n+^{9}C strength for them to be observed in the pickup reactions.

Arguments for assigning the 2^+ and 4^+ members of the 0_2^+ band is ^{10}Be were based on the reduced width γ_α^2 for α decay [19, 52]. For the 2^+ state of this band, taking the weighted mean of the α+^{6}He$_{g.s.}$ branching ratios from Refs. [50, 52] and the tabulated total decay width [30], the partial decay is Γ_α=14.5(37) keV. With a standard channel radius of a_α=1.6 fm$\times$($A_1^{1/2}$ + $A_2^{1/3}$), the reduced width is $\gamma_\alpha^2 = \frac{\Gamma_\alpha}{2P_2}$ = 0.56(25) MeV where P_2 is the ℓ=2 barrier penetration factor. This reduced width is quite large and close to the Wigner limit [53] of $\gamma_{\alpha W}^2 = \frac{3\hbar^2}{2\mu a_\alpha^2}$=0.88 MeV. For the analog state in ^{10}C assigned in this work, we obtain γ_α^2= 0.16(7) MeV from a similar analysis using the total decay width and branching ratio from Table I. Alternatively using the more precise total width measurement of Γ=190(35) keV from Ref. [54], we obtain γ_α^2=0.17(3) MeV. These values are still significant, but are below the value for the analog state. For the three observed decay channels of this ^{10}C state, the dimensionless reduced decay widths are γ_p^2/γ_{pW}^2=0.03(1), $\gamma_{2p}^2/\gamma_{2pW}^2$= 0.09(4), and $\gamma_\alpha^2/\gamma_{\alpha W}^2$=0.19(9) where the $2p$ decay is treated as the emission of a diproton with de-

cay energy of E_{p-p}=0.9 MeV which is the average E_{p-p} value in Fig. 17(a). Of these channels, α decay is the strongest, consistent with an α-cluster structure of the internal wavefunction.

Let us now turn our attention to the 4^+ members in these analog 0_2^+ rotational bands. From the partial α+^{6}He$_{g.s.}$ decay width of Γ=0.13(1) MeV [19], the reduced width of the 4_1^+ state in ^{10}Be is γ_α^2=0.15(1) MeV close to the value for the 2^+ state in ^{10}C. For the proposed 4^+ analog state in ^{10}C, using the branching ratio uncorrected for detector efficiency in Table I, we obtain γ_α^2=0.10(2) MeV. Of course the efficiency correction is unknown providing some extra uncertainty to this result, but we see the reduced decay width is of similar magnitude to its analog. Thus the α decay widths of these 2^+ and 4^+ states in ^{10}C support our contention that they are members of the 0_2^+ rotational band.

From an extrapolation of the lower-energy members using the best-fit momentum of inertia, we expect the 6^+ member of this 0_2^+ band in ^{10}C to lie at E^* ≈14.5 MeV. The 15.95-MeV state is closest to this expectation. However for a spin of 6^+, its reduced α-decay width would be only γ_α^2=0.024(6) MeV without correcting for detector efficiencies. The detector-efficiency corrections are unlikely to significantly increase this value bringing it closer to those obtained for the 2^+ and 4^+ states. Thus this state is probably not the 6^+ member and we would expect the real 6^+ state is probably quite wide making it difficult to observed.

B. α-cluster states in ^{11}N

The case for the α-cluster structure of the $3/2_2^-$ state in ^{11}N should also be considered. In the mirror nucleus ^{11}Be, Bohlen *et al* have tentatively assigned members of the K=$3/2^-$ band up to spin $19/2^-$ [47] though definite spin assignments have only been made for the first two members. The moment of inertia of this tentative band is quite large consistent with α-cluster structure. However from a theoretical study, Descouvemont suggested the $3/2^-$ and $5/2^-$ states do not have α-cluster structure [55]. But assuming that there is a K=$3/2^-$ band, can we assign excited members from this work to the ^{11}N counterpart? If, like the 0_2^+ band in ^{10}C, the lower members would all have two-proton decay branches, then these states should show up in the $2p$+^{9}B$_{g.s.}$ invariant-mass spectrum of Fig. 10(b) where three other peaks (O, P and Q) in addition to the $3/2^-$ state are observed. Assuming these are all members of the K=$3/2^-$ band, we compare their rotational curve to that given by Bohlen *et al.* for ^{11}Be in Fig. 19. The degree of overlap of the two tentative bands is remarkable. We note that the presence of these peaks in the $2p$+^{9}B$_{g.s.}$ invariant-mass distribution does not guarantee they has a prompt $2p$ decay branch as sequential decays through ^{10}C intermediate states are possible and indeed the E^*=7.476-MeV state has some p+^{10}C$_{2_2^+}$ branch (peak R). The higher members are above the α-decay threshold, but identifying the α+^{7}B decay is almost impossible given the large ^{7}B$_{g.s.}$ decay width of Γ=0.8 MeV [30]. Although the data is quite suggestive, further work is needed to shore up these tentative α-cluster bands in both ^{11}Be and ^{11}N.

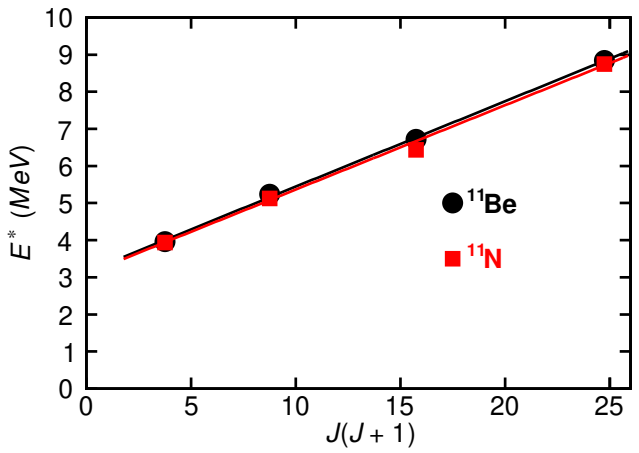

FIG. 19. Spin dependence of tentative K=$3/2^-$ rotational bands in the mirror nuclei ^{11}Be and ^{11}N. The levels for ^{11}Be are taken from Bohlen et al. [47] while the levels for ^{11}N are those observed in the $2p$+^{9}B$_{g.s.}$ spectrum of this work. The red and black lines, which almost completely overlap, are fits to the two sets of levels.

C. $2n$ decay of neutron-rich cluster configurations

Given the observation of $2p$ decay from the proton-rich α-cluster configurations, one may consider the possibility of $2n$ decay of their neutron-rich cousins. In Fig. 18, where the ^{10}Be and ^{10}C rotational bands are displayed, we have also shown the thresholds for p, $2p$, and α decay of ^{10}C and their analogs for the neutron-rich counterparts. The 0^+ and 2^+ states in the ^{10}Be 0_2^+ band are below the $2n$ decay threshold thus leaving the 4^+ state as the first possibility for $2n$ decay in ^{10}Be. Note the $2p$ threshold is below the α threshold for ^{10}C, while the $2n$ threshold is above the α threshold for ^{10}Be. The energetics for $2n$ decay would be more favorable in ^{12}Be where ^{6}He+^{6}He and α+^{8}He decays of molecular states have been observed [18, 56, 57]. The thresholds for these decays, 10.1 and 8.9 MeV, respectively, are quite large compared to the $2n$ decay threshold of 3.7 MeV.

VI. CONCLUSIONS

Highly-fragmented decay channels of ^{10}C and ^{11}N excited states have been studied using invariant-mass data from four previous experiments involving both inelastic scattering, multi-nucleon knockout, and neutron pickup reactions. For the $2p$+2α exit channel, states in ^{10}C could be separated by gating and vetoing on the ground states of ^{8}Be and ^{9}B observed in the invariant mass of the 2α and p+2α subevents. These very narrow states are

the only intermediate resonances in the subevents that can be cleanly identified without significant underlying background. The excitation-energy spectra associated with the ≈100-keV-wide resonances, ^{6}Be$_{g.s.}$ and the $5/2^{-}$ state in ^{9}B, could also be isolated with a more indirect technique. Identification of states associated with even wider intermediate states was not possible. These techniques were also applied to the $3p$+2α decay channel of ^{11}N for which previously unknown states were observed.

A number of democratic $2p$ emitters were identified in the ^{10}C and ^{11}N states associated with α-cluster structure. In particular, we have tentatively identified the first three members of the excited 0^{+}_{2} band in ^{10}C with all observed members showing some probability for $2p$ emission. The large moment-of-inertia of this band is very similar to that for the analog structure in the mirror ^{10}Be and the 2^{+} and 4^{+} members, which are above the α threshold, also have large reduced widths for α decay. The spins of the first two members were deduced from comparison of the momentum correlations measured for their $2p$ branches to known 0^{+} and 2^{+} two-proton emitters of similar mass.

A second $3/2^{-}$ state was observed in ^{11}N which $2p$ decays to the ground state of ^{9}B. Possibly this state has a strong α-cluster structure which would be associated with a K=$3/2^{-}$ rotational band. We have tentatively identified all members of this band up to J=$9/2^{-}$. These members have very similar excitation energies to their counterparts in the mirror nucleus ^{11}Be proposed by Bohlen *et al.* [47].

Two more $2p$ emitters were observed in ^{11}N at E^{*}=9.271(58) and 11.047(67) MeV. Both of these states $2p$ decay to the lowest $5/2^{-}$ intermediate state of ^{9}B. The momentum correlations in these cases are also consistent with the results for ^{12}O$_{g.s.}$ and ^{16}Ne$_{g.s.}$, but the significance of this is not clear as the $2p$ decay energy of these two ^{11}N states are significantly larger than those for the ground-state emitters. Further work is needed to constrain the structure of these states.

ACKNOWLEDGMENTS

This material is based upon work supported by the U.S. Department of Energy, Office of Science, Office of Nuclear Physics under award numbers DE-FG02-87ER-40316. We thank Simin Wang for fruitful discussions.

[1] O. Bochkarev, L. Chulkov, A. Korsheninniicov, E. Kuz'min, I. Mukha, and G. Yankov, Democratic decay of ^{6}Be states, Nucl. Phys. A **505**, 215 (1989).

[2] M. Pfützner, M. Karny, L. V. Grigorenko, and K. Riisager, Radioactive decays at limits of nuclear stability, Rev. Mod. Phys. **84**, 567 (2012).

[3] L. Grigorenko, T. Wiser, K. Miernik, R. Charity, M. Pftzner, A. Banu, C. Bingham, M. wiok, I. Darby, W. Dominik, J. Elson, T. Ginter, R. Grzywacz, Z. Janas, M. Karny, A. Korgul, S. Liddick, K. Mercurio, M. Rajabali, K. Rykaczewski, R. Shane, L. Sobotka, A. Stolz, L. Trache, R. Tribble, A. Wuosmaa, and M. Zhukov, Complete correlation studies of two-proton decays: ^{6}Be and ^{45}Fe, Phys. Lett. B **677**, 30 (2009).

[4] S. M. Wang and W. Nazarewicz, Puzzling two-proton decay of ^{67}Kr, Phys. Rev. Lett. **120**, 212502 (2018).

[5] S. M. Wang, W. Nazarewicz, R. J. Charity, and L. G. Sobotka, Structure and decay of the extremely proton-rich nuclei ^{11,12}O, Phys. Rev. C **99**, 054302 (2019).

[6] S. M. Wang, W. Nazarewicz, R. J. Charity, and L. G. Sobotka, Nucleon-nucleon correlations in the extreme oxygen isotopes (2021), arXiv:2108.08007 [nucl-th].

[7] I. A. Egorova, R. J. Charity, L. V. Grigorenko, Z. Chajecki, D. Coupland, J. M. Elson, T. K. Ghosh, M. E. Howard, H. Iwasaki, M. Kilburn, J. Lee, W. G. Lynch, J. Manfredi, S. T. Marley, A. Sanetullaev, R. Shane, D. V. Shetty, L. G. Sobotka, M. B. Tsang, J. Winkelbauer, A. H. Wuosmaa, M. Youngs, and M. V. Zhukov, Democratic decay of ^{6}Be exposed by correlations, Phys. Rev. Lett. **109**, 202502 (2012).

[8] K. W. Brown, R. J. Charity, L. G. Sobotka, L. V. Grigorenko, T. A. Golubkova, S. Bedoor, W. W. Buhro, Z. Chajecki, J. M. Elson, W. G. Lynch, J. Manfredi, D. G. McNeel, W. Reviol, R. Shane, R. H. Showalter, M. B. Tsang, J. R. Winkelbauer, and A. H. Wuosmaa, Interplay between sequential and prompt two-proton decay from the first excited state of ^{16}Ne, Phys. Rev. C **92**, 034329 (2015).

[9] T. B. Webb, R. J. Charity, J. M. Elson, D. E. M. Hoff, C. D. Pruitt, L. G. Sobotka, K. W. Brown, J. Barney, G. Cerizza, J. Estee, G. Jhang, W. G. Lynch, J. Manfredi, P. Morfouace, C. Santamaria, S. Sweany, M. B. Tsang, T. Tsang, S. M. Wang, Y. Zhang, K. Zhu, S. A. Kuvin, D. McNeel, J. Smith, A. H. Wuosmaa, and Z. Chajecki, Particle decays of levels in ^{11,12}N and ^{12}O investigated with the invariant-mass method, Phys. Rev. C **100**, 024306 (2019).

[10] M. F. Jager, R. J. Charity, J. M. Elson, J. Manfredi, M. H. Mahzoon, L. G. Sobotka, M. McCleskey, R. G. Pizzone, B. T. Roeder, A. Spiridon, E. Simmons, L. Trache, and M. Kurokawa, Two-proton decay of ^{12}O and its isobaric analog state in ^{12}N, Phys. Rev. C **86**, 011304(R) (2012).

[11] K. W. Brown, W. W. Buhro, R. J. Charity, J. M. Elson, W. Reviol, L. G. Sobotka, Z. Chajecki, W. G. Lynch, J. Manfredi, R. Shane, R. H. Showalter, M. B. Tsang, D. Weisshaar, J. R. Winkelbauer, S. Bedoor, and A. H. Wuosmaa, Two-proton decay from the isobaric analog state in ^{8}B, Phys. Rev. C **90**, 027304 (2014).

[12] R. J. Charity, J. M. Elson, J. Manfredi, R. Shane, L. G. Sobotka, Z. Chajecki, D. Coupland, H. Iwasaki, M. Kilburn, J. Lee, W. G. Lynch, A. Sanetullaev, M. B. Tsang, J. Winkelbauer, M. Youngs, S. T. Marley, D. V. Shetty, A. H. Wuosmaa, T. K. Ghosh, and M. E. Howard, $2p$-$2p$ decay of ^{8}**C** and isospin-allowed $2p$ decay of the isobaric-analog state in ^{8}**B**, Phys. Rev. C **82**, 041304(R) (2010).

[13] R. J. Charity, J. M. Elson, J. Manfredi, R. Shane, L. G. Sobotka, B. A. Brown, Z. Chajecki, D. Coupland, H. Iwasaki, M. Kilburn, J. Lee, W. G. Lynch, A. Sanetullaev, M. B. Tsang, J. Winkelbauer, M. Youngs, S. T.

Marley, D. V. Shetty, A. H. Wuosmaa, T. K. Ghosh, and M. E. Howard, Investigations of three-, four-, and five-particle decay channels of levels in light nuclei created using a ^{9}C beam, Phys. Rev. C **84**, 014320 (2011).

[14] K. W. Brown, R. J. Charity, J. M. Elson, W. Reviol, L. G. Sobotka, W. W. Buhro, Z. Chajecki, W. G. Lynch, J. Manfredi, R. Shane, R. H. Showalter, M. B. Tsang, D. Weisshaar, J. R. Winkelbauer, S. Bedoor, and A. H. Wuosmaa, Proton-decaying states in light nuclei and the first observation of ^{17}Na, Phys. Rev. C **95**, 044326 (2017).

[15] R. J. Charity, T. D. Wiser, K. Mercurio, R. Shane, L. G. Sobotka, A. H. Wuosmaa, A. Banu, L. Trache, and R. E. Tribble, Continuum spectroscopy with a ^{10}C beam: Cluster structure and three-body decay, Phys. Rev. C **80**, 024306 (2009).

[16] R. B. Wiringa, S. C. Pieper, J. Carlson, and V. R. Pandharipande, Quantum Monte Carlo calculations of A=8 nuclei, Phys. Rev. C **62**, 014001 (2000).

[17] W. von Oertzen, Dimers based on the α+α potential and chain states of carbon isotopes, Z. Phys. A **357**, 355 (1997).

[18] M. Freer, J. C. Angélique, L. Axelsson, B. Benoit, U. Bergmann, W. N. Catford, S. P. G. Chappell, N. M. Clarke, N. Curtis, A. D'Arrigo, E. de Goes Brennard, O. Dorvaux, B. R. Fulton, G. Giardina, C. Gregori, S. Grévy, F. Hanappe, G. Kelly, M. Labiche, C. Le Brun, S. Leenhardt, M. Lewitowicz, K. Markenroth, F. M. Marqués, M. Motta, J. T. Murgatroyd, T. Nilsson, A. Ninane, N. A. Orr, I. Piqueras, M. G. Saint Laurent, S. M. Singer, O. Sorlin, L. Stuttgé, and D. L. Watson, Exotic molecular states in ^{12}Be, Phys. Rev. Lett. **82**, 1383 (1999).

[19] M. Freer, E. Casarejos, L. Achouri, C. Angulo, N. I. Ashwood, N. Curtis, P. Demaret, C. Harlin, B. Laurent, M. Milin, N. A. Orr, D. Price, R. Raabe, N. Soić, and V. A. Ziman, $\alpha : 2n : \alpha$ molecular band in ^{10}Be, Phys. Rev. Lett. **96**, 042501 (2006).

[20] M. Wallace, M. Famiano, M.-J. van Goethem, A. Rogers, W. Lynch, J. Clifford, F. Delaunay, J. Lee, S. Labostov, M. Mocko, L. Morris, A. Moroni, B. Nett, D. Oostdyk, R. Krishnasamy, M. Tsang, R. de Souza, S. Hudan, L. Sobotka, R. Charity, J. Elson, and G. Engel, The high resolution array (HiRA) for rare isotope beam experiments, Nucl. Instrum. Methods A **583**, 302 (2007).

[21] K. Mercurio, R. J. Charity, R. Shane, L. G. Sobotka, J. M. Elson, M. Famiano, A. H. Wuosmaa, A. Banu, C. Fu, L. Trache, R. E. Tribble, and A. M. Mukhamedzhanov, Correlated two-proton decay from ^{10}C, Phys. Rev. C **78**, 031602(R) (2008).

[22] L. V. Grigorenko, T. D. Wiser, K. Mercurio, R. J. Charity, R. Shane, L. G. Sobotka, J. M. Elson, A. H. Wuosmaa, A. Banu, M. McCleskey, L. Trache, R. E. Tribble, and M. V. Zhukov, Three-body decay of ^{6}Be, Phys. Rev. C **80**, 034602 (2009).

[23] K. W. Brown, R. J. Charity, L. G. Sobotka, Z. Chajecki, L. V. Grigorenko, I. A. Egorova, Y. L. Parfenova, M. V. Zhukov, S. Bedoor, W. W. Buhro, J. M. Elson, W. G. Lynch, J. Manfredi, D. G. McNeel, W. Reviol, R. Shane, R. H. Showalter, M. B. Tsang, J. R. Winkelbauer, and A. H. Wuosmaa, Observation of long-range three-body Coulomb effects in the decay of ^{16}Ne, Phys. Rev. Lett. **113**, 232501 (2014).

[24] R. J. Charity, K. W. Brown, J. Elson, W. Reviol, L. G. Sobotka, W. W. Buhro, Z. Chajecki, W. G. Lynch, J. Manfredi, R. Shane, R. H. Showalter, M. B. Tsang, D. Weisshaar, J. Winkelbauer, S. Bedoor, D. G. McNeel, and A. H. Wuosmaa, Invariant-mass spectroscopy of ^{18}Ne, ^{16}O, and ^{10}C excited states formed in neutron-transfer reactions, Phys. Rev. C **99**, 044304 (2019).

[25] R. J. Charity, K. W. Brown, J. Okołowicz, M. Płoszajczak, J. M. Elson, W. Reviol, L. G. Sobotka, W. W. Buhro, Z. Chajecki, W. G. Lynch, J. Manfredi, R. Shane, R. H. Showalter, M. B. Tsang, D. Weisshaar, J. R. Winkelbauer, S. Bedoor, and A. H. Wuosmaa, Invariant-mass spectroscopy of ^{14}O excited states, Phys. Rev. C **100**, 064305 (2019).

[26] T. B. Webb, S. M. Wang, K. W. Brown, R. J. Charity, J. M. Elson, J. Barney, G. Cerizza, Z. Chajecki, J. Estee, D. E. M. Hoff, S. A. Kuvin, W. G. Lynch, J. Manfredi, D. McNeel, P. Morfouace, W. Nazarewicz, C. D. Pruitt, C. Santamaria, J. Smith, L. G. Sobotka, S. Sweany, C. Y. Tsang, M. B. Tsang, A. H. Wuosmaa, Y. Zhang, and K. Zhu, First observation of unbound ^{11}O, the mirror of the halo nucleus ^{11}Li, Phys. Rev. Lett. **122**, 122501 (2019).

[27] T. B. Webb, R. J. Charity, J. M. Elson, D. E. M. Hoff, C. D. Pruitt, L. G. Sobotka, K. W. Brown, J. Barney, G. Cerizza, J. Estee, W. G. Lynch, J. Manfredi, P. Morfouace, C. Santamaria, S. Sweany, M. B. Tsang, T. Tsang, Y. Zhang, K. Zhu, S. A. Kuvin, D. McNeel, J. Smith, A. H. Wuosmaa, and Z. Chajecki, Invariant-mass spectrum of ^{11}O, Phys. Rev. C **101**, 044317 (2020).

[28] R. J. Charity, L. G. Sobotka, and J. A. Tostevin, Single-nucleon knockout cross sections for reactions producing resonance states at or beyond the drip line, Phys. Rev. C **102**, 044614 (2020).

[29] R. J. Charity, T. B. Webb, J. M. Elson, D. E. M. Hoff, C. D. Pruitt, L. G. Sobotka, K. W. Brown, G. Cerizza, J. Estee, W. G. Lynch, J. Manfredi, P. Morfouace, C. Santamaria, S. Sweany, C. Y. Tsang, M. B. Tsang, Y. Zhang, K. Zhu, S. A. Kuvin, D. McNeel, J. Smith, A. H. Wuosmaa, and Z. Chajecki, Observation of the exotic isotope ^{13}F located four neutrons beyond the proton drip line, Phys. Rev. Lett. **126**, 132501 (2021).

[30] (2021), evaluated Nuclear Structure Data File (ENSDF), http://www.nndc.bnl.gov/ensdf/.

[31] A. M. Lane and R. G. Thomas, R-matrix theory of nuclear reactions, Rev. Mod. Phys. **30**, 257 (1958).

[32] T. Goigoux, P. Ascher, B. Blank, M. Gerbaux, J. Giovinazzo, S. Grévy, T. Kurtukian Nieto, C. Magron, P. Doornenbal, G. G. Kiss, S. Nishimura, P.-A. Söderström, V. H. Phong, J. Wu, D. S. Ahn, N. Fukuda, N. Inabe, T. Kubo, S. Kubono, H. Sakurai, Y. Shimizu, T. Sumikama, H. Suzuki, H. Takeda, J. Agramunt, A. Algora, V. Guadilla, A. Montaner-Piza, A. I. Morales, S. E. A. Orrigo, B. Rubio, Y. Fujita, M. Tanaka, W. Gelletly, P. Aguilera, F. Molina, F. Diel, D. Lubos, G. de Angelis, D. Napoli, C. Borcea, A. Boso, R. B. Cakirli, E. Ganioglu, J. Chiba, D. Nishimura, H. Oikawa, Y. Takei, S. Yagi, K. Wimmer, G. de France, S. Go, and B. A. Brown, Two-proton radioactivity of ^{67}Kr, Phys. Rev. Lett. **117**, 162501 (2016).

[33] L. V. Grigorenko and M. V. Zhukov, Two-proton radioactivity and three-body decay. ii. exploratory studies of lifetimes and correlations, Phys. Rev. C **68**, 054005 (2003).

[34] K. Miernik, W. Dominik, Z. Janas, M. Pfützner, L. Grigorenko, C. R. Bingham, H. Czyrkowski, M. Ćwiok, I. G. Darby, R. Dabrowski, T. Ginter, R. Grzywacz, M. Karny, A. Korgul, W. Kuśmierz, S. N. Liddick, M. Rajabali, K. Rykaczewski, and A. Stolz, Two-proton correlations

in the decay of ^{45}Fe, Phys. Rev. Lett. **99**, 192501 (2007).
[35] S. M. Wang and W. Nazarewicz, Fermion pair dynamics in open quantum systems, Phys. Rev. Lett. **126**, 142501 (2021).
[36] H. T. Fortune and R. Sherr, Structure of ^{16}Ne ground state, Phys. Rev. C **66**, 017301 (2002).
[37] L. V. Grigorenko, T. A. Golubkova, and M. V. Zhukov, Thomas-Ehrman effect in a three-body model: The ^{16}Ne case, Phys. Rev. C **91**, 024325 (2015).
[38] P. G. Sharov, L. V. Grigorenko, A. N. Ismailova, and M. V. Zhukov, Pauli-principle driven correlations in four-neutron nuclear decays, JETP Lett. **110**, 5 (2019).
[39] H. T. Fortune and R. Sherr, Constraints on energy of ^{9}B$(1/2^{+})$ and ^{10}C(0^{+}_{2}), Phys. Rev. C **73**, 064302 (2006).
[40] T. D. Baldwin, W. N. Catford, D. Mahboub, C. N. Timis, N. I. Ashwood, N. M. Clarke, N. Curtis, V. Ziman, T. A. D. Brown, S. P. Fox, B. R. Fulton, D. Groombridge, D. L. Watson, V. F. E. Pucknell, and D. C. Weisser, First excited $\frac{1}{2}^{+}$ state in ^{9}B, Phys. Rev. C **86**, 034330 (2012).
[41] H. Fortune, Narrow resonances in ^{11}N and ^{15}F, Nucl. Phys. A **968**, 342 (2017).
[42] K. T. Schmitt, K. L. Jones, A. Bey, S. H. Ahn, D. W. Bardayan, J. C. Blackmon, S. M. Brown, K. Y. Chae, K. A. Chipps, J. A. Cizewski, K. I. Hahn, J. J. Kolata, R. L. Kozub, J. F. Liang, C. Matei, M. Matoš, D. Matyas, B. Moazen, C. Nesaraja, F. M. Nunes, P. D. O'Malley, S. D. Pain, W. A. Peters, S. T. Pittman, A. Roberts, D. Shapira, J. F. Shriner, M. S. Smith, I. Spassova, D. W. Stracener, A. N. Villano, and G. L. Wilson, Halo nucleus ^{11}Be: A spectroscopic study via neutron transfer, Phys. Rev. Lett. **108**, 192701 (2012).
[43] D. Morrissey, K. McDonald, D. Bazin, B. Brown, R. Harkewicz, N. Orr, B. Sherrill, G. Souliotis, M. Steiner, J. Winger, S. Yennello, B. Young, S. Lukyanov, G. Chubarian, and Y. Oganessian, Single neutron emission following ^{11}Li β-decay, Nucl. Phys. A **627**, 222 (1997).
[44] A. Bonaccorso, F. Cappuzzello, D. Carbone, M. Cavallaro, G. Hupin, P. Navrátil, and S. Quaglioni, Application of an ab initio S matrix to data analysis of transfer reactions to the continuum populating ^{11}Be, Phys. Rev. C **100**, 024617 (2019).
[45] N. Itagaki and S. Okabe, Molecular orbital structures in ^{10}Be, Phys. Rev. C **61**, 044306 (2000).
[46] M. Lyu, Z. Ren, B. Zhou, Y. Funaki, H. Horiuchi, G. Röpke, P. Schuck, A. Tohsaki, C. Xu, and T. Yamada, Investigation of ^{10}Be and its cluster dynamics with the nonlocalized clustering approach, Phys. Rev. C **93**, 054308 (2016).
[47] H. Bohlen, A. Blazevič, B. Gebauer, W. Von Oertzen, S. Thummerer, R. Kalpakchieva, S. Grimes, and T. Massey, Spectroscopy of exotic nuclei with multi-nucleon transfer reactions, Prog. Part. Nucl. Phys. **42**, 17 (1999).
[48] H. G. Bohlen, W. von Oertzen, R. Kalpakchieva, B. Gebauer, S. M. Grimes, A. Lenz, T. N. Massey, M. Milin, C. Schulz, T. Kokalova, S. Torilov, and S. Thummerer, Structure of neutron-rich Be and C isotopes, Phys. At. Nucl. **66**, 1494 (2003).
[49] S. Hamada, M. Yasue, S. Kubono, M. H. Tanaka, and R. J. Peterson, Cluster structures in ^{10}Be from the ^{7}Li$(\alpha$,p$)^{10}$Be reaction, Phys. Rev. C **49**, 3192 (1994).
[50] M. Milin, M. Zadro, S. Cherubini, T. Davinson, A. Di Pietro, P. Figuera, D. Miljanić, A. Musumarra, A. Ninane, A. Ostrowski, M. Pellegriti, A. Shotter, N. Soi, and C. Spitaleri, Sequential decay reactions induced by a 18 MeV ^{6}He beam on ^{6}Li and ^{7}Li, Nucl. Phys. A **753**, 263 (2005).
[51] D. Brink, Kinematical effects in heavy-ion reactions, Phys. Lett. B **40**, 37 (1972).
[52] J. A. Liendo, N. Curtis, D. D. Caussyn, N. R. Fletcher, and T. Kurtukian-Nieto, Near threshold three-body final states in ^{7}Li+^{7}Li reactions at $E_{\rm lab} = 34$MeV, Phys. Rev. C **65**, 034317 (2002).
[53] T. Teichmann and E. P. Wigner, Sum rules in the dispersion theory of nuclear reactions, Phys. Rev. **87**, 123 (1952).
[54] M. J. Schneider, B. W. Ridley, M. E. Rickey, J. J. Kraushaar, and W. R. Zimmerman, Study of unbound levels in ^{10}C via ^{10}B$(^{3}$He$, t)$, Phys. Rev. C **12**, 335 (1975).
[55] P. Descouvemont, Microscopic study of α clustering in the ^{9,10,11}Be isotopes, Nucl. Phys. A **699**, 463 (2002).
[56] R. J. Charity, S. A. Komarov, L. G. Sobotka, J. Clifford, D. Bazin, A. Gade, Jenny Lee, S. M. Lukyanov, W. G. Lynch, M. Mocko, S. P. Lobastov, A. M. Rogers, A. Sanetullaev, M. B. Tsang, M. S. Wallace, S. Hudan, C. Metelko, M. A. Famiano, A. H. Wuosmaa, and M. J. van Goethem, Particle decay of ^{12}Be excited states, Phys. Rev. C **76**, 064313 (2007).
[57] A. Saito, A. Shimoura, Y. U. Matsuyama, H. Baba, N. Aoi, T. Gomi, Y. Higurashi, K. Ieki, N. I. N. Imai, S. Hanno, S. Kubono, M. Kunibu, S. Michimasa, T. Motobayashi, T. Nakamura, H. Ryuto, H. Sakurai, M. Serata, E. Takeshita, S. Takeuchi, T. Teranishi, K. Ue, K. Yamada, and Y. Yanagisawa, The ^{6}He+^{6}He and α+^{8}He cluster states in ^{12}Be via α-inelastic scattering, Mod. Phys. Lett. A **24**, 1858 (2010).